Rotational velocities of low-mass stars in the Pleiades and Hyades

Donald M. Terndrup[1], John R. Stauffer[2], Marc H. Pinsonneault[1], Alison Sills[1], Yongquan Yuan[1], Burton F. Jones[3], Debra Fischer[4], and Anita Krishnamurthi[5]

ABSTRACT

We have obtained high-resolution spectra of 89 M dwarf members of the Pleiades and Hyades and have derived radial velocities, Hα equivalent widths, and spectroscopic rotational velocities for these stars. Typical masses of the newly-observed Pleiades and Hyades stars are $\sim 0.4M_{\odot}$ and $\sim 0.2M_{\odot}$, respectively. We combine our new observations with previously published data to explore the rotational evolution of young stars with $M \leq 0.4M_{\odot}$. The average rotation rate in the Hyades (age 600 Myr) is about 0.4 that of the Pleiades (110 Myr), and the mean equivalent widths of Hα are also lower. As found in previous studies, the correlation between rotation and chromospheric activity is identical in both clusters, implying that the lower activity in the Hyades is a result of the lower rotation rates. We show that a simple scaling of the Pleiades rotational distribution for $M \leq 0.4M_{\odot}$, corrected for the effects of structural evolution, matches that of the Hyades if the average angular momentum loss from the Pleiades to the Hyades age is factor of ≈ 6. This suggests that the distribution of initial angular momenta and disk-locking lifetimes for the lowest mass stars was similar in both clusters. We argue that this result provides further evidence for a saturation of the angular momentum loss rate at high rotational velocities.

Subject headings: stars: rotation, magnetic fields — open clusters and associations: individual (Pleiades, Hyades)

1. Introduction

The rotational properties of stars, and how those properties evolve with time, are a strong function of mass. Somewhat less obviously, our knowledge of those properties is also a function

[1]Department of Astronomy, The Ohio State University, Columbus, OH 43210.

[2]Smithsonian Astrophysical Observatory, 60 Garden Street, Cambridge, MA 02138.

[3]Lick Observatory, Board of Studies in Astronomy and Astrophysics, University of California, Santa Cruz, CA 95064.

[4]Department of Astronomy, University of California, Berkeley, CA 94720.

[5]JILA, University of Colorado and National Institute of Standards and Technology, Campus Box 440, Boulder, CO 80303.

of mass because lower mass stars are fainter and thus more difficult to observe. For four decades (Slettebak 1956; Abt & Hunter 1962), we have known that B and A stars usually have large rotational velocities, and that there there is little evidence for angular momentum loss on the main sequence in this mass range. The mean rotational velocity decreases rapidly towards lower mass within the F spectral class, and there is evidence for main sequence spindown, particularly for late-F dwarfs (Kraft 1967; Wolff & Simon 1997). The correspondence in the location of this rotational velocity break with the appearance of the Ca II HK lines in emission led Skumanich (1972) to associate both phenomena with the development of an outer convective zone. Non-radiative processes within the convection zone lead to a temperature reversal above the photosphere and to a steady-state wind which carries away angular momentum by coupling to the stellar magnetic field, thus explaining the observed main sequence spindown (e.g., MacGregor & Brenner 1991).

A good empirical understanding of the rotational velocity evolution of main sequence G and K dwarfs has only been obtained during the past two decades (Stauffer et al. 1984, 1985, 1989, 1991a; Soderblom et al. 1993; Allain et al. 1996; Bouvier et al. 1997; Jones et al. 1997; Krishnamurthi et al. 1998; Queloz et al. 1998). These observations show that most stars in this mass range arrive on the main sequence as relatively slow rotators, but that a significant fraction (about 20-25%) arrive on the main sequence as rapid rotators with $20 < v \sin i < 200$ km s^{-1}. Based on observations of open clusters of different ages, the time scale for these rapid rotators to lose most of their angular momentum ranges from tens to hundreds of millions of years, with the time scale increasing with decreasing stellar mass (e.g., Stauffer et al. 1987; Chaboyer et al. 1995). In order to be consistent with these observations, theoretical evolutionary models require one or more of the following features: core-envelope rotational decoupling (Endal & Sofia 1981; Pinsonneault et al. 1990; Allain 1998), coupling of the stellar rotation to that of its circumstellar disk during pre-main sequence evolution (Königl 1991; Li & Cameron 1993), or saturation of the angular momentum loss rate above a specified rotation rate (Keppens et al. 1995). The expectations from theory will be discussed at greater length in § 4.

The most recent observational efforts have been to extend the available spectroscopic data to lower $v \sin i$ limits (Delfosse et al. 1998; Queloz et al. 1998) and to lower masses, approaching the limiting mass for hydrogen burning in a few cases. Jones et al. (1996) and Oppenheimer et al. (1997) have determined rotational velocities for a small sample of stars in the the Pleiades and Hyades with masses down to $\sim$0.1 $M_{\odot}$. Basri & Marcy (1995) and Delfosse et al. (1998) have similarly obtained rotational velocities for very low mass field stars. In addition, there have been many studies of the rotation periods of stars in young clusters as revealed from photometry (e.g., Allain et al. 1996; Bouvier 1996; Choi & Herbst 1996; Patten & Simon 1996; Kearns et al. 1997; Kearns & Herbst 1998; Krishnamurthi et al. 1998; Barnes et al. 1999; Stassun et al. 1999; Terndrup et al. 1999, and references in these papers). All of these studies indicate that the time scale for angular momentum loss is longer for lower mass stars, with stars near 0.1 $M_{\odot}$ having significant rotation rates even after stars at higher masses have all spun down. This facet of the observational database is best explained by assuming that the critical rotation rate for saturation of the angular momentum loss

rate is a decreasing function of mass, a conclusion supported by measures of chromospheric and coronal activity in these stars (Patten & Simon 1996; Bouvier et al. 1997; Krishnamurthi et al. 1998).

In this paper, we provide new spectroscopic rotational velocities ($v \sin i$) for 89 M dwarfs in the Pleiades and Hyades. When combined with previously published data for these clusters, we can explore the distribution of rotation rates in these two clusters much better than in the past, particularly for low-mass stars (here $M \leq 0.4 M_{\odot}$). We also analyze the strength of Hα emission in the two clusters, and discuss implications of our data for theoretical modeling of angular momentum loss.

2. Observations and Data Reduction

2.1. Target Selection and Observations

Our new spectral data were obtained during three observing runs: Nov. 19-21, 1996 on the KPNO 4m telescope[6], Dec. 4-5, 1996 on the Keck I telescope[7] using the HIRES spectrograph (Vogt et al. 1994), and again on Dec. 4-5, 1997 with the same setup. At KPNO, we used the echelle spectrograph and the red long camera, a slit width of 1.0 arcsec, a 31.6 lines/mm grating, and a Tektronix 2048^2 CCD, resulting in an instrumental resolution of about 37000 and wavelength coverage from 6000 to 8700 Å. With HIRES, we used the standard echelle grating, a 0.86×14 arcsecond slit, and a Tektronix 2048×2048 CCD with 24-micron pixels for a spectral resolution of about 45000 and wavelength coverage from 6300 to 8700 Å. We used standard IRAF tools to do the basic CCD data processing and also the order extraction, sky subtraction and wavelength calibration. At both telescopes, exposure times were selected in order to obtain S/N ~ 10 near blaze center around 6600 Å (for Hα); given the redness of the program stars, this generally resulted in S/N $\sim 15 - 20$ near blaze center for orders around 8500 Å.

In the Pleiades, spectroscopic rotational velocities have previously been obtained for a large, reasonably unbiased sample of stars down to $V \sim 14$ (Soderblom et al. 1993; Queloz et al. 1998). Below $V = 14$ ($M \simeq 0.6 M_{\odot}$), however, the fraction of known members with measured rotational velocities decreases rapidly. Even for the stars with existing $v \sin i$ measures, most are from an "early" program (in the 1980's) with somewhat poorer spectral resolution resulting in $v \sin i$ limits of $9 - 10$ km s^{-1} for the slow rotators in the cluster (cf. Stauffer & Hartmann 1987). In order to obtain a better determination of the distribution of rotational velocities for $M < 0.6 M_{\odot}$, we

[6]Kitt Peak National Observatory, NOAO, is operated by the Association of Universities for Research in Astronomy, Inc., under cooperative agreement with the National Science Foundation.

[7]The W. M. Keck Observatory is operated as a scientific partnership among the the California Institute of Technology, the University of California and the National Aeronautics and Space Administration. The Observatory was made possible by the generous financial support of the W. M. Keck Foundation.

devoted one of the KPNO 4m runs to obtain spectra of Pleiades members with published $BVRI$ photometry in the magnitude range $14 < V < 17$. We succeeded in obtaining spectra of 59 of these stars during the KPNO run. A small set of additional spectra for stars in this magnitude range was obtained during a 1997 Keck HIRES run, bringing the total number of Pleiads with new spectral data to 71.

In the Hyades, our goal was to constrain better the rotational velocity distribution for (Cousins) $V - I_C > 3.0$. Poor weather in Hawaii during the time of our observing run significantly impaired the success of our efforts, but we did manage to obtain spectra of 18 Hyades members redder than $V - I_C = 2.9$.

Typical spectra in the region of Hα and at $\sim$8400 Å for fast, moderate, and slowly rotating Pleiades members from the KPNO run are shown in Figure 1, and a similar set of spectra for Hyades members from the Keck observing run are shown in Figure 2. Note the systematic change in the Hα profile as the rotational velocity increases.

2.2. Radial and Rotational Velocity Analysis

Radial and rotational velocities for all of the program stars were derived using the cross-correlation package developed by R. Hewett and L. Hartmann, as described in Hartmann et al. (1986); see Jones et al. (1997) and Stauffer et al. (1997a,b) for other recent papers which have used this package. Briefly, a high signal-to-noise spectrum of a slowly rotating star of similar spectral type to the program objects is chosen as a template. For a given spectral type, two or more orders of the echelle spectra are chosen where there is a good set of intrinsically narrow, moderate strength absorption features in the program objects, and where there are few or no terrestrial (Earth atmosphere) features. The program star spectra for these echelle orders are then cross-correlated against the template star spectrum, and the width and location of the cross-correlation peak derived. The calibration of this width to yield an estimate of $v \sin i$ is determined by convolving the spectrum of another high signal-to-noise slow rotator with rotational broadening functions for a range of $v \sin i$ and then cross-correlating those artificially broadened spectra versus the template star spectrum.

In all cases, we used high signal-to-noise spectra of Gliese (1969) catalog M dwarfs as the calibrators. For the KPNO spectra, we used Gl 851 as the template star, and Gl 15B as the "spin-up" star; for the Keck spectra, we used spectra of Gl 905 and Gl 402 for these purposes. These slow rotators have rotation rates which are considerably smaller than our limit in this study: Gl 15B has $v \sin i < 3.1$ km s^{-1}, Gl 402 has $v \sin i < 2.3$ km s^{-1}, Gl 905 has $v \sin i < 1.2$ km s^{-1} (Delfosse et al. 1998), and Gl 851 has $v \sin i = 2.5$ km s^{-1} (Marcy & Chen 1992). To determine the rotational velocities of the slow rotators amongst our program stars, we used echelle orders dominated by TiO bands for the cross-correlation analysis; for rapid rotators, we used echelle orders with several strong, relatively isolated atomic absorption features. We also cross-correlated a portion of an order

dominated by Earth-atmosphere O_2 lines to correct for drifts in the spectrograph zero-point.

As a test of the radial velocity stability of the Keck HIRES, we observed five M dwarf radial velocity standards from Marcy & Benitz (1989). One of these (Gl 402) was used as our cross-correlation template star; the mean shift of the other four relative to the tabulated Marcy & Benitz value was -0.12 km s^{-1} with a one sigma dispersion of only 0.3 km s^{-1}. This shows that radial velocities accurate to better than a half kilometer per second can be achieved with HIRES with no special effort, at least for slow rotators (for example, we only used standard spectral extraction routines and did not take ThAr spectra except at the beginning and end of the night). The expected accuracy of the derived radial and rotational velocities decreases with increasing rotational velocity, with one sigma errors for both quantities being of order 10% of the $v \sin i$ based on our previous experience and on comparison of our measurements for different echelle orders. This characteristic of the radial velocity errors can be readily seen in Figure 3, which plots the radial velocity against $v \sin i$ for (upper panel) our sample in the Pleiades and (lower panel) in the Hyades. In the Pleiades sample, which contains a number of rapidly rotating stars, the scatter about the mean radial velocity is larger for the rapidly rotating stars. In addition to a higher scatter, there is some indication that the radial velocities for the most rapidly rotating stars are underestimated by 3–4 km s^{-1}. That the scatter about the mean at all velocities is within the expected errors (10% of $v \sin i$) leads us to conclude that few, if any, of our sample are not members of these clusters as judged by their radial velocities.

The radial and rotational velocities for the Pleiades stars are complied in Tables 1 (KPNO data) and 2 (Keck data), along with Hα equivalent widths (below) and cross references to each star in various catalogs. For most of these stars, the Cousins photometry displayed in these two tables has been transformed from measured Kron $V - I_K$ colors using the coefficients measured by (Bessell & Weis 1987). Colors marked with a colon are transformed from lower-quality photographic magnitudes tabulated by Hambly et al. (1993). Hyades data are shown in Table 3.

Our radial velocities agree very well with previous determinations of the mean velocities of much brighter stars in these clusters, which are shown as dashed lines in the two panels of Figure 3. For the Pleiades, we find $\langle V_r \rangle = 6.0 \pm 0.3$ km s^{-1} (error of the mean), in agreement with the value of 5.97 ± 0.07 km s^{-1} derived by Narayanan & Gould (1999) in their analysis of Pleiades stars with parallaxes from Hipparcos. For the Hyades, our new radial velocities average to $\langle V_r \rangle = 39.7 \pm 0.4$ km s^{-1}, close to the value of 39.2 ± 0.2 km s^{-1} for Hipparcos-selected stars within 20 pc from the Hyades cluster center (Perryman et al. 1998), and also in agreement with $\langle V_r \rangle = 37.9 \pm 1.3$ km s^{-1} for non-binary dM stars in that cluster (Stauffer et al. 1997b). A better estimate of the accuracy of the velocities in the Hyades can be made by comparing them to the Stefanik & Latham (1985) model of the dependence of velocity on position, using their convergent point and Hyades space motion. We find a scatter of 0.68 km s^{-1}, which reduces to 0.50 km s^{-1} if two stars with the largest velocity differences (Re 119 and Re 158) are excluded.

2.3. Additional Spectral Analysis

For each of the program objects, we have measured the shape and equivalent width of Hα. Two or three of the stars have essentially no feature at Hα; all of the rest have Hα in emission. For the slowest rotators, the emission line profiles are steep-sided and boxy, with a central reversal; the profiles gradually change to centrally peaked and approximately Gaussian in shape for the most rapid rotators, as illustrated in Figures 1 and 2. The equivalent widths, which are given as positive values, range from barely detectable (0.1 Å) to moderately strong ($\sim$ 6 Å). Two of the Pleiades dMe stars have Hα equivalent widths of $\sim$ 9 Å, but we suspect that their steady-state chromospheric emission level is less than this and that the equivalent width we have measured has been enhanced due to a flare.

Jones et al. (1996) noted that two or three of the Pleiades dMe stars they observed had broad Hα wings in addition to the normal Hα emission profile seen in the other Pleiades stars. They speculated that these broad wings might be caused by mass motions produced during flares. We have reobserved two of those stars during the current program, and do not find such wings on the new spectra. The measured Hα equivalent widths for the new spectra are lower than for the previous spectra, in accord with the idea that the broad wings may be associated with flares (i.e., the stars were flaring during the previous observations). In addition, we have found two new Pleiades dMe stars in our new set of spectra which show broad Hα wings similar to what had been found by Jones et al. The stars from the current program with broad Hα wings are HCG 143 (= T19B) and HGC 277 (= T105). Both of these stars have larger than average Hα equivalent widths but fairly average rotational velocities.

Finally, we have examined all of our spectra to check for the presence of a detected lithium 6708 Å absorption feature. Because of the relatively low S/N of our spectra, we generally would not detect lithium absorption lines with equivalent width less than about 100 mÅ. We do detect lithium in two of our program objects - HII 1756 ($V = 14.1$, $V - I_C = 1.63$, W_λ(Li) = 150 mÅ) and HCG 75 ($V = 14.45$, $V - I_C = 1.81$, W_λ(Li) = 110 mÅ). Both stars are at the extreme blue end of our target list. They are comparable in effective temperature to the latest type main sequence stars in which lithium has previously been detected (García-López et al. 1994; Jones et al. 1996), and have comparable equivalent widths to those stars. Both stars are slow rotators ($v \sin i \leq 7$ km s^{-1}and $v \sin i = 8$ km s^{-1}, respectively).

3. Analysis

3.1. Effective Temperatures

We now proceed to adopt an effective temperature scale for the stars in our sample. The goal here is to combine our new data with previous measures of $v \sin i$ in the Pleiades and Hyades (§ 3.3, below). The photometry for these stars is heterogeneous, with some having only $B - V$ colors,

others having only $V - I_C$, and a subset having both colors. We thus need temperature estimates on a common scale for both colors.

Effective temperatures are derived from fitting a new generation of the Yale Rotating Evolution Code (YREC) isochrones (Guenther et al. 1992) to the color-magnitude diagram of the Pleiades. The new models, which include the effects of rotation, are fully described by Sills et al. (1999); they incorporate many improvements from a number of groups to calculations of low-temperature stellar atmospheres, opacities and equations of state. By including the physics of many molecules, Allard & Hauschildt (1995) have created model atmospheres which are valid for low mass stars with effective temperatures less than 4000 K. The equation of state of Saumon et al. (1995) includes partial dissociation and ionization of hydrogen and helium caused by both pressure and temperature effects, and is applicable to both low mass stars and giant planets. Finally, Alexander & Ferguson (1994) added atomic line absorption, molecular line absorption and some grain absorption and scattering to the usual sources of continuous opacity to produce opacity tables which reach temperatures as low as 700 K. Since most previous atmospheres, opacities and equations of state did not include the effects of molecules and grains, these three improvements significantly increase our ability to model the interior physics of very low mass stars (also see Chabrier & Baraffe 1997).

Isochrones were generated by computing evolutionary tracks at mass intervals of $0.05 M_\odot$, and using linear interpolation between the time points. The zero-point for the age scale was set to the deuterium-burning birthline as given by Palla & Stahler (1991). The manner in which these isochrones were fit to the Pleiades data is illustrated in Figure 4, which plots dereddened photometry for a compilation of stars with previous $v \sin i$ measures (discussed in § 3.3 below) for which $B - V$ photometry is available. The photometry has been dereddened using $E(B - V) = 0.04$, which is appropriate for most regions of the Pleiades (Breger 1986; Stauffer & Hartmann 1987). The dashed line in Figure 4 displays an isochrone for an age of 110 Myr, which was chosen as an average between recent estimates using isochrones (e.g., Meynet et al. 1993) and the somewhat higher values derived from the detection of Li at low temperatures (Stauffer et al. 1998b). (Our analysis is insensitive to the exact choice of the Pleiades age, since the mass-luminosity relationship is a very slow function of age near 110 Myr). We adopted the metallicity of the Pleiades as solar; Boesgaard & Friel (1990), for example, derived $[\mathrm{Fe/H}] = -0.034 \pm 0.024$ for this cluster.

In generating the Pleiades isochrone, the Allard & Hauschildt (1995) model atmospheres were used as a boundary condition (pressure at $T = T_{\rm eff}$) on the interior models. We chose to employ the empirical Yale color calibration (Green et al. 1987) to generate model colors instead of relying on the color-temperature relations of Allard & Hauschildt (1995). The two color calibrations have similar problems in matching the photometry. Both predict colors which are far too blue for the lowest-mass stars, though the match in $V - I_C$ is somewhat better in the Allard & Hauschildt (1995) calibration, though not as good in $B - V$ for hotter stars. We chose to adjust the color-temperature calibration under the restricted assumption that the errors were entirely in the color-temperature calibration and not in the bolometric corrections (cf. Jeffries & Tolley 1998). The approach used here is discussed at greater length by Pinsonneault et al. (2000).

The solid line in Figure 4 is the same isochrone adjusted to match the photometry better, as follows: For $(B-V)_0 \leq 0.75$, the isochrone was used to determine the distance to the Pleiades using a method discussed at length by Pinsonneault et al. (1998). In this method, the distance modulus for each star is computed by differencing the dereddened magnitude with the absolute magnitude of the isochrone. This produces a distribution of distance moduli which is strongly peaked at the mean distance to the cluster, but which has a tail toward shorter distances for the binary stars. The derived distance was taken as the median distance modulus for stars with $(B-V)_0 \leq 0.75$ and within 0.2 mag of this peak; for the Pleiades, this yields a distance modulus of $(m - M_{\rm V})_0 = 5.6$. For $(B-V)_0 \leq 0.75$, the YREC isochrone fits the lower envelope of the Pleiades photometry quite well, indicating that the model atmosphere colors and bolometric corrections are accurate in this temperature range.

For $(B-V)_0 > 0.75$, we assumed that the YREC isochrone produced the correct effective temperature and luminosity, and that the Yale bolometric correction was also correct in this temperature range. For cooler temperatures, we assumed that any differences between the Pleiades photometry and the isochrone was caused by an incorrect transformation between effective temperature and color; thus the adjustment process shifts a star of a given mass in color but does not change its magnitude. The isochrone was adjusted horizontally by determining intervals of color which corresponded to mass intervals of 0.1 $M_\odot$, measuring the distribution of distance moduli for stars in those color intervals with respect to the isochrone, then shifting the isochrone to require that the median distance modulus be the same as derived for the stars with $(B-V)_0 \leq 0.75$. (If the unadjusted isochrone were too blue, for example, then it would lie below the photometry, and the derived distances would be too low). Down to $(B-V)_0 = 1.5$, the required color shifts are small, everywhere less than 0.065 mag. We shall now refer to the adjusted YREC isochrone as the "empirical" isochrone for the Pleiades.

In Figure 5, we display the YREC and empirical isochrones in $(V-I)_0$ compared to available photometry (these are not always the same stars as in Figure 4). The symbols are the same as in Figure 4, except we have added the $V-I$ photometry for the stars in this paper (open triangles). The production of the empirical isochrone in this color (i.e., the determination of horizontal shifts to the unadjusted isochrone to match the photometry) used the same method as in $B-V$. A reddening of $E(V-I_C) = 0.06$ was used, computed from $E(B-V)$ using the relations in Bessell & Brett (1988). Here the color shifts are significantly larger for stars at the faint end of the main sequence, corresponding to $\Delta(V-I)_0 = 0.5$ mag at $M = 0.25 M_\odot$.

The empirical isochrone was used to generate transformations between $(B-V)_0$ or $(V-I)_0$ and effective temperature for stars in the Pleiades. These are shown in Figure 6, which shows the $B-V$ transformation in the lower panel and that in $V-I$ above. The solid line in each panel shows the color-temperature relation for the empirical isochrone. In the lower panel, the dashed line shows the color-$T_{\rm eff}$ calibration discussed in Soderblom et al. (1993) for $(B-V)_0 \leq 1.35$; this is very slightly cooler than the empirical isochrone. In the upper panel, the dashed line shows the temperature scale for K and M dwarfs employed by Stauffer et al. (1997a), which is is based on the

Bessell (1979) color transformations for warmer stars and the Kirkpatrick et al. (1993) observations of M dwarfs. The filled points are the measured effective temperatures for individual M dwarfs in Kirkpatrick et al. (1993). The match between the temperature scale for the empirical isochrone and that of Kirkpatrick et al. is very good for the lowest masses ($T_{\rm eff} = 3200$ K, which corresponds to $M \approx 0.1 M_{\odot}$), even though – as we saw in Figure 5 – a rather large adjustment in color was needed to match the Pleiades photometry. The open points in Figure 6 show temperatures derived by Leggett et al. (1996) for nearby M dwarfs; their temperature scale is about 100 K cooler than that of Kirkpatrick et al. (1993). As discussed by Stauffer et al. (1998a), the best effective temperature scale for the Pleiades is probably intermediate between the two. The temperatures in $V-I$ adopted here are considerably warmer (up to 100 K) at intermediate temperatures than that in Stauffer et al. (1997a); this is partly a consequence of adopting an older age for the Pleiades than the value of 70 Myr used in that paper, and partly a consequence of using different isochrones.

We computed effective temperatures for Pleiades stars independently from $(B-V)_0$ and $(V-I)_0$, using the relations shown in Figure 6. For stars with $(B-V)_0 > 1.35$, only the $(V-I)_0$ color was used. If both colors were available, the two temperatures were averaged. The use of the empirical isochrone assures that the temperatures from both colors will be consistent with one another. For stars with photometry in both colors, the mean difference in temperature between the two estimates was $\langle T_{\rm eff}(B-V) - T_{\rm eff}(V-I) \rangle = -27$ K (i.e., the scale from $(V-I)_0$ was slightly hotter), with a scatter of 110 K r.m.s. Photometric errors of about 0.03 in either color would produce this scatter in the derived temperatures.

We also generated an isochrone appropriate for the Hyades, using the new YREC models for [Fe/H] = +0.13 (Boesgaard & Friel 1990), an age of 600 Myr (Perryman et al. 1998), and a distance modulus of 3.34 (Perryman et al. 1998; Pinsonneault et al. 1998), and then applying the same shifts in color which were generated from matching the photometry in the Pleiades. The reddening adopted here was $E(B-V) = 0.0$ (Crawford & Perry 1966). The Hyades cannot itself be used to calibrate the color-temperature relation, because there is a significant dispersion in distance for stars in the cluster. Pinsonneault et al. (1998) compare the YREC isochrones to Hyades stars with Hipparcos parallaxes, which are all much brighter than the stars in our sample. The match between the isochrones and the photometry is very good.

3.2. Mass estimates

Because the Pleiades and Hyades are not coeval and have different metallicities, the relationship between effective temperature and stellar mass is not identical for the two clusters. Consequently, a comparison of the rotation rates for the two data sets is sometimes better made in mass rather than effective temperature or color.

We derived mass estimates for the stars in our sample using polynomial fits between mass and $V - I_C$ for the Pleiades and Hyades empirical isochrones described previously. The aim here was

to adopt a color-temperature relation (rather than a luminosity-mass relation) so that binary stars would not be assigned higher masses than single stars of the same observed color. For $M < 0.4M_{\odot}$, the Hyades stars are, on average, about 90 K cooler at each mass than stars in the Pleiades. On this scale, the typical mass of the newly observed Pleiades stars is 0.4 $M_{\odot}$, and is 0.2 $M_{\odot}$ in the Hyades.

For the faintest, reddest stars in both clusters, the method used to estimate masses based on effective temperature produces masses which are systematically too low (i.e., substellar) compared to other estimates in the literature for such faint stars. We have therefore considered an alternative procedure which relies more on a star's luminosity rather than its inferred temperature. For this alternative method, we adopte the Monet et al. (1992) estimate of the I-band bolometric correction. Using the available I_C photometry, we then computed the bolometric magnitude for each star. Then we derived the mass by interpolation using the empirical isochrones for the two clusters. For $M \geq 0.25M_{\odot}$, the two methods gave the save average relation between color and mass, though the mass estimates could differ considerably for probable binaries, where the latter method yields a higher mass because of the brighter I_C magnitude. Below $M = 0.25M_{\odot}$, the alternative method yielded higher masses, with the coolest stars in both clusters having mass estimates in the range 0.12–0.15 $M_{\odot}$, in accord with masses estimated for these stars in previous papers (Stauffer et al. 1994, 1995). In order to avoid assigning substellar masses for the reddest stars, we adopted a compromise mass scale, taking the masses from the empirical isochrones for $M \geq 0.25M_{\odot}$, and smoothly interpolating to the alternative mass scale for lower masses. As we are mainly concerned with broad trends in the rotational properties with stellar mass, , in particular by discussing the stars in intervals of mass (below), none of the details of our analysis depend sensitively on the adopted mass scale.

3.3. Distribution of rotational velocities

In Figure 7, we plot the $v \sin i$ data for the Pleiades (upper panel) and the Hyades (lower panel) against effective temperature. The solid points in this figure are for the stars in this paper, while open points are for additional data in the literature for the Pleiades (Basri & Marcy 1995; Queloz et al. 1998) and for the Hyades (Stauffer et al. 1997b). In the Hyades, no additional rotation rates from the literature are plotted for $\log(T_{\rm eff}) > 3.6$, which corresponds to $V - I_C < 1.9$; in this temperature range, Ziskin (1993) detected no stars with $v \sin i > 10$ km s^{-1} (the limiting velocity in that study) up to $T \approx 6000$ K, except for some tidally locked binaries (see also Thorburn et al. 1993). Studies of the rotation periods of Hyades stars earlier than spectral type K7 also show that all are rotating slowly (Radick et al. 1987). At the bottom of each panel of Figure 7, we have also indicated the stellar masses from the Pleiades and Hyades empirical isochrone, derived as described previously.

Our new data increases the number of stars with spectroscopic measures of rotation for $M < 0.5M_{\odot}$. Our goals here are twofold: to compare the rotational distribution of low-mass stars to

the well-studied sample of stars near solar mass, and to explore the characteristics of angular momentum loss at the bottom of the main sequence. As discussed more extensively in § 4, the range of rotation rates present at each mass sets strong constraints on the mechanisms for angular momentum loss on the main sequence and earlier.

The distribution of rotation rates in the Pleiades has a strong dependence on mass. For $M > 0.9 M_{\odot}$, most stars fall near a lower envelope which is a decreasing function of mass, going from ≈ 30 km s^{-1} at $M = 1.25 M_{\odot}$ to ≈ 8 km s^{-1} from 0.6 – 0.9 $M_{\odot}$. At higher masses there is a wide distribution of rotation rates from $v \sin i \leq 7$ km s^{-1} up to $v \sin i \approx 100$ km s^{-1}, a factor of at least 15 in angular momentum per unit mass. Most of the stars in this mass range are slowly rotating, with $v \sin i \sim 7$ km s^{-1}, but there is also a small fraction of stars with quite rapid rotation ($v \sin i \approx 80$ km s^{-1}), producing an apparently bimodal distribution of rotation rates. The range of rotation rates declines to lower masses: below about 0.3 $M_{\odot}$, there are few or no stars with upper limits on $v \sin i$ (typically 7 km s^{-1}), and the upper envelope of the rotation rates is decreasing with decreasing stellar mass. It would also seem that the distribution of rotation rates changes 0.5 $M_{\odot}$, in that the distribution is uniform and not bimodal, as found at higher masses (cf. Jones et al. 1996). This flat distribution is quite unlike the distribution expected for a narrow range of rotation rates broadened by random inclination angle, which would be peaked toward stars with high apparent rotation. The full range of rotation rates near 0.2 $M_{\odot}$ is only about a factor of 3–4. The fall in the upper envelope of rotation rates corresponds to a fairly constant maximum *angular* rotation rate, since the stellar radius declines with decreasing mass (this is shown in Fig. 6 of Jones et al. 1996).

In Figure 8, we present histograms of the distribution rotational rates, arranged in three groups from highest to lowest masses (top to bottom). The histograms show the number of stars per intervals of $\Delta \log_{10}(v \sin i) = 0.151$ (i.e., intervals of $\sqrt{2}$ in $v \sin i$). Stars with limits on $v \sin i$ are plotted in the bin corresponding to the limiting value; the bins in each histogram were constructed so that the stars which have $v \sin i \leq 7$ km s^{-1} in this study would be plotted in the leftmost bin. The mass ranges used in each histogram are shown; the upper limit for the highest mass bin was set to exclude stars in that part of the $v \sin i$ distribution where the average velocities are increasing with higher temperature. In addition, the distribution of velocities for our combined Hyades sample is shown as a dashed histogram in the lowest panel of the Figure.

Although there are some Pleiades stars in all bins of $v \sin i$ for $M \geq 0.4$ $M_{\odot}$, the separation between the majority slow-rotator group and the fast-rotators is apparent in the upper two panels of Figure 8. In these mass bins, the fast rotators have a peak in the distribution of velocities near $v \sin i \approx 80$ km s^{-1}. The peak of velocities for the slow rotators is only a few km s^{-1} for the hottest stars shown; it possibly rises to about $7 - 9$ km s^{-1} for the interval $0.4 < (M/M_{\odot}) < 0.6$, though this is less certain because many of the slowest rotators in this mass range have limits on $v \sin i$.

The data in the lower panel of Figure 8 show that the lowest mass stars have a flat distribution of rotational velocities. There is no evidence for the bimodal distribution observed for higher mass

stars. The distribution of velocities is remarkable also in that there are few stars rotating at or below the observational limit in this study. A similar lack of slow rotators has been seen in other young clusters (Allain et al. 1996). The Hyades still has a number of stars with limits on the velocity, at least down to $M \sim 0.2\ M_{\odot}$. Because of the number of stars with limits in the Hyades, it is not possible to estimate accurately if the range of velocities is much larger than the factor of 3–4 in the Pleiades, though it is certainly not as small as would be produced by a very narrow rotation distribution viewed at random inclination angles.

3.4. Hα emission

Figure 9 shows the correlation between the equivalent width of Hα and stellar temperature. Stars in the Pleiades are shown as open symbols, while those in the Hyades are displayed as filled symbols. The Pleiades data come from this study and from Jones et al. (1996). The Hyades points come from this paper, Stauffer et al. (1997b) and Jones et al. (1996). The different symbols indicate the source of the data, as outlined in the figure caption. In the case where we reobserved stars from earlier work, only the Hα value from this paper is plotted.

In both clusters, the well known trend towards higher Hα widths at lower temperatures is readily seen. The distribution of Hα for the Hyades hardly overlaps at all with that of the Pleiades: the maximum equivalent width at each temperature for the Hyades is about equal to the minimum in the Pleiades. Thus we see a decline in chromospheric activity with cluster age (cf. Caillaut 1996). Note that the strong rise of Hα equivalent widths towards cooler temperatures is mainly an effect of the rapidly falling continuum near the Hα line; the stars actually have a falling luminosity in Hα with temperature (cf. Young et al. 1989; Basri & Marcy 1995), consistent with the picture sketched above that the rate of angular momentum loss is declining with decreasing stellar mass.

Figure 10 shows the correlation between $v \sin i$ and Hα for the Pleiades and Hyades stars plotted in Figure 9. The masses have been derived from the empirical isochrone, and the stars have been divided so that each bin contains approximately the same number of stars. The scale for all three panels is identical. At all temperatures, the Hα rises only slowly with rotation, except for slow rotation rates where the rise with rotation is much steeper. Such a change in slope is more evident when the ratio of rotation speed to the convective overturn time is considered (Patten & Simon 1996; Krishnamurthi et al. 1998), and has been used to argue that the magnetic field strength and angular momentum loss rate saturate at higher rotation rates. In the bottom panel of Figure 10, which shows the data for the lowest temperatures, there is a significant number of both Hyades and Pleiades stars. There are some stars in both clusters with Hα width considerably higher than the mean value, which may represent stars which were flaring at the time of observation. With the exception of these points, the correlation between rotation and chromospheric activity is identical for both clusters. This means that the average Hα strength and the average rotation rate decline with age by the same factor. It is thus not correct to use the Hα strengths as a direct indicator of age as occasionally has been proposed in the literature; we see here that stars of a factor of 5.5

different in age are indistinguishable if they have the same rotation rates. It is still true, however, that one can use the distribution of Hα vs. color as an age indicator, since this relies on the mass dependence of spindown times as well as the chromospheric response (cf. Stauffer et al. 1997a).

4. Discussion: The evolution of rotation rates at low mass

While our new data do not push the study of rotation into new territory – rapid rotation at low stellar masses has been seen before – they do provide a larger statistical sample at low masses. The most important aspect of the data is that we have actual measures of $v \sin i$, rather than just limits, for most low-mass stars in the Hyades. This provides us with the chance to explore the nature of and time scale for angular momentum loss over the age range sampled by the two clusters ($\approx$ 110 to 600 Myr).

In particular, we pose this question: can we expect that the rotational distribution of low mass stars in the Pleiades will evolve to look like that of the Hyades when the former cluster is a factor of ≈ 5.5 older? If we can, then we provide independent support for the current paradigm employed in theoretical models of angular momentum evolution (Krishnamurthi et al. 1997, and references therein). If not, then we may be uncovering evidence that the conditions of early stellar evolution (initial angular momentum or lifetimes of stellar disks) differed in the two clusters, or that the current evolutionary paradigm is inadequate. Sills et al. (1999) provide a direct comparison between theory and the available data in these and other young clusters.

There are four principal ingredients of the current theoretical paradigm: (1) Young stars begin their lives as fully convective objects; because the time scale for convective transport is much smaller than that for angular momentum loss, the stars rotate as solid bodies[8] and their angular momentum profile with depth is fully specified by the surface rotation rate, which is typically modeled to be like that of T Tauri stars (Choi & Herbst 1996). (2) For some time the surface rotation periods of the stars, now contracting toward the main sequence, are held nearly constant by magnetic fields threading between the star and its circumstellar disk (Königl 1991; Cameron & Campbell 1993; Cameron et al. 1995; Keppens et al. 1995). When the disk and star decouple, the surface rotation rate rises as the star continues its contraction. (3) Angular momentum loss continues via a magnetized wind during the evolution to the main sequence and well into the early main sequence lifetime. In a linear dynamo the angular momentum loss rate is proportional to the cube of the surface angular velocity (Weber & Davis 1967; Kawaler 1988). The resulting spindown for the rapid rotators would, however, take place on such a short time scale as to be in conflict with the maximum rotation rates seen in young clusters (Pinsonneault et al. 1990). Observational data on the correlation between chromospheric and coronal activity suggest that there exists a saturation

[8]What matters for the internal transport of angular momentum is the radial dependence of rotation. The models we are using do not handle latitudinal circulation. In the Sun, the convection zone shows latitudial differential rotation, but this is nearly constant with radial depth (e.g., Thompson et al. 1996).

threshold which reduces the angular momentum loss rate at rapid rotation (Noyes et al. 1984; Patten & Simon 1996; Krishnamurthi et al. 1998). (4) At any period in the evolution, the surface rotation rates can also depend on the mechanism of and time scale for internal angular momentum transport. For stars with significant radiative cores, this may result in a core and surface which spin at different rates. Since the size of the radiative core depends on the stellar mass and the location of the star along an evolutionary track, there are stellar masses and cluster ages where the differences between solid-body and differentially rotating models are more pronounced (Krishnamurthi et al. 1997).

The existence of the fast rotators at higher masses requires both that some stars are tied to their disks for only a short time ($\leq$ 1 Myr) and that the rotational spindown is saturated above some threshold. This latter property is usually modeled as

$$\frac{dJ}{dt} = -K_\omega \omega \omega_{\rm crit}^2, \quad \omega > \omega_{\rm crit} \tag{1}$$

$$= -K_\omega \omega^3, \quad \omega \leq \omega_{\rm crit} \tag{2}$$

where J is the angular momentum, ω the angular rotation rate, and $\omega_{\rm crit}$ is the angular rotation rate where saturation occurs. The observation that the upper envelope of the rotational distribution rises to lower masses for $M \geq 0.6 M_\odot$ (Fig. 7) is typically modeled by having the saturation threshold be a function of mass (e.g., Krishnamurthi et al. 1997), with saturation occurring at slower angular velocities in lower-mass stars, which then experience less angular momentum loss early on (Barnes & Sofia 1996).

Modeling the rotation rates in young clusters is not free of ambiguities because the various ingredients of the current paradigm are not independent. In particular, the production of a dispersion of rotation rates at a given mass could be the result of a dispersion in initial angular momentum or in disk-locking lifetimes. The normal approach (Krishnamurthi et al. 1997; Sills et al. 1999) is to start all stars with a fixed initial angular spin rate, set by observations of T Tauri stars, and subsequently to produce a dispersion by a distribution of disk lifetimes. There is a degeneracy between the derived $\omega_{\rm crit}$ and the assumed initial rotation rates at the stellar birthline: if very young stars have higher rotation rates than those usually taken, as indicated by the recent observations in Orion by Stassun et al. (1999), then higher values of $\omega_{\rm crit}$ are required. (The Stassun et al. paper also demonstrates that there exists a wide range of rotation periods even at an age of 1 Myr.)

Here we can ignore the issue of what produces the dispersion in rotation rates at low masses, instead focusing on how this dispersion would change with time. The models of Sills et al. (1999) predict that stars with $M \leq 0.4 M_\odot$ should still be rotating with $\omega \geq \omega_{\rm crit}$ even at the age of the Hyades, because without saturation of the loss law all the stars would be rotating at lower rates than is observed. Now the angular momentum can be written as $J = I\omega$, where I is the momentum of inertia. If I is a constant or varies much more slowly with time than ω, then in the saturated case we have

$$\frac{1}{\omega}\frac{d\omega}{dt} = -\frac{K_\omega}{I}\omega_{\rm crit}^2, \tag{3}$$

which has the solution $\omega(t) = \omega_0 e^{-at}$, where a is a constant, taking $\omega \rightarrow 0$ as $t \rightarrow \infty$. Thus once $\omega_{\rm crit}$ is set (though it can vary with mass), all stars of a given mass will spin down by the same factor over an interval of time, and the ratio of $v \sin i$ between the fastest and slowest spinners will be constant. Alternatively, if all stars were spinning with $\omega < \omega_{\rm crit}$, we would have

$$\frac{d\omega}{dt} = -\frac{K_\omega}{I}\omega^3, \tag{4}$$

which has the solution $\omega(t) \propto t^{-1/2}$. With the passage of time, the rapid rotators would experience greater loss, and the ratio of $v \sin i$ between the fastest and slowest spinners will decline.

The data in Figures 7 and 8 show that the range of rotation at the lowest masses is similar in both clusters (specifically, we concluded that the range in rotation in the Hyades is at least as large as in the Pleiades). This supports the idea that the appropriate value of $\omega_{\rm crit}$ for these stars has to be sufficiently low that even the slow spinners in the Hyades still have $\omega \geq \omega_{\rm crit}$. In this case, we should be able to find a constant q (where $0 \leq q \leq 1$) to scale the Pleiades velocity distribution from the observed $N(v \sin i)d(v \sin i)$ so that $N(qv \sin i)d(v \sin i)$ matches the observed distribution in the Hyades (here we mean that the shape of the velocity distributions would be identical). The value of q would then calibrate the constant K_ω in equations 1 and 2. This turns out not to be possible without correcting for fact that the lowest mass stars in the Pleiades are still contracting towards the main sequence. For example (using the isochrones discussed in § 3.1), the radii of Hyades stars with $M = 0.2 M_\odot$ are 0.8 that of the Pleiades, and the mass where Hyades stars are on the main sequence is close to $0.5 M_\odot$. Were there no angular momentum loss, the low-mass Pleiads would spin up as they contracted, and would have higher rotation rates at the age of the Hyades. That the rates in the Hyades are, in fact, about a factor of two lower than in the Pleiades indicates that the angular momentum loss is larger than any increase in rotation rates during the contraction.

We modeled the future evolution of the Pleiades stars as follows. At each mass M, let $r_i(M)$ be the radius at the age of the Pleiades, and $r_f(M)$ be the radius at the age of the Hyades. If the contraction towards the main sequence is homologous, then the moment of inertia I would scale as r^2. Conservation of angular momentum requires $I\omega = $ const., and so we should expect the rotation rates to increase by a factor of $(r_i/r_f)^2$ in the absence of loss. Then, if as argued above, there should be a constant factor q reduction in the observed rotation rates from angular momentum loss, a Pleiades star currently observing at a rate of $v_i = v \sin i$ will be have $v \sin i = q v_i (r_i/r_f)^2$ at the age of the Hyades.

We calculated an expected (future) distribution for the Pleiades by computing the factors $(r_i/r_f)^2$ for each star, using the masses derived from the empirical isochrones. Then the resulting rotation rates were reduced by a factor q, but were set to a minimum value of $v \sin i = 6$ km s^{-1} to match the limits in our current study. For each q, we used a K-S test to compare the cumulative distribution $F(v \sin i)$ of scaled Pleiades velocities to that in the Hyades. Values outside the range $0.10 \leq q \leq 0.23$ could be excluded at the 95% confidence level; the best match was achieved for $q = 0.17$, for which the probability that the two distributions could be drawn from the same sample

was $P_{\rm KS} = 0.90$. We illustrate the good match which results from this computation in Figure 11, where thick line shows the observed cumulative distribution in the Hyades, while the thin line shows the distribution of scaled velocities in the Pleiades.

This exercise sets a average time scale for the angular momentum loss below $m = 0.4 M_{\odot}$. The factor of six loss in the angular momentum between the age of the Pleiades and that of the Hyades means that the e-folding time scale for loss is near 250 Myr for $M \leq 0.4 M_{\odot}$ (the range of f excluded by the K-S test corresponds to an estimated average time scale of 245 ± 55 Myr). This would imply that the fastest rotators in the Hyades, now spinning near $v \sin i = 30$ km s^{-1}, would have undetectable rotation rates after 1-2 billion years.

The similarity in the shapes of the two distributions in Figure 11 shows that the distribution of initial rotation rates for low-mass stars in the two clusters must not have been very different, and provides a verification of the existence of saturation in the angular momentum loss at high rotation rates. This also explains the change in the distribution of rotation rates near $M = 0.5 M_{\odot}$: at higher masses, the rotation rates fall below $\omega_{\rm crit}$ by the age of the Hyades, if they are not already so at the age of the Pleiades. We therefore see a reduction in the range of rotation rates by the age of the Hyades, which would not be the case if all stars had $\omega > \omega$crit.

At present, only a few young clusters have sufficiently large samples at these low masses (Sills et al. 1999) for comparison to the Pleiades and Hyades. Data in other clusters could potentially show that the distribution of initial rotation rates was universal or that it depends on cluster mass, stellar density, binary fraction, or other factors. A more detailed comparison of the current data with theoretical models of angular momentum evolution might allow a better calibration of $\omega_{\rm crit}$ for low-mass stars. This may remove some of the current ambiguities in the modeling, specifically between the disk-locking lifetime and the initial rotation rates.

JRS acknowledges support from NASA Grants NAGW-2698 and NAGW-3690. DT and MHP acknowledge support from NASA Grants NAG5-7150 and NSF grant AST-9731621. AS acknowledges support from NSERC. We are grateful to the referee, who made many valuable suggestions.

REFERENCES

Abt, H. & Hunter, J. 1962, ApJ, 136, 381

Alexander, D. R., & Ferguson, J. W. 1994, ApJ, 437, 879

Allain, S. 1998, A&A, 333, 629

Allain, S., Bouvier, J., Prosser, C., Marschall, L., & Laaksonen, B. 1996, A&A, 305, 498

Allard, F., & Hauschildt, P. H. 1995, ApJ, 445, 433

Barnes, S., & Sofia, S. 1996, ApJ, 462, 746

Barnes, S. A., Sofia, S., Prosser, C. F., & Stauffer, J. R. 1999, ApJ, 516, 263

Basri, G., & Marcy, G. 1995, AJ, 109, 762

Bessell, M. S. 1979, PASP, 91, 589

Bessell, M. S., & Brett, J. M. 1988, PASP, 100, 1134

Bessell, M. S., & Weis, E. W. 1987, PASP, 99, 642

Boesgaard, A. M., &Friel, E. D. 1990, ApJ, 351, 467

Bouvier, J. 1996, A&AS, 120, 127

Bouvier, J., Forrestini, M., & Allain, S. 1997, A&A, 326, 1023

Breger, M. 1986, ApJ, 309, 311

Bryja, C., Humphreys, R. M., & Jones, T. J. 1994, AJ, 107, 246

Caillaut, J.-P. 1996, in Cool Stars, Stellar Systems, and the Sun, 9th Cambridge Workshop, ed. R. Pallavicini and A. K. Dupree, ASP. Conf. Ser. 109, 325

Cameron, A. C., Campbell, C., & Quaintrell, H. 1995, A&A, 298, 133

Cameron, A. C., & Campbell, C. G. 1993, A&A, 274, 309

Chaboyer, B., Demarque, P., & Pinsonneault, M. H. 1995, ApJ, 441, 876

Chabrier, G., & Baraffe, I. 1997, A&A, 327, 1039

Choi, P., & Herbst, W. 1996, AJ, 111, 283

Crawford, D., & Perry, C. 1966, AJ, 71, 206

Delfosse, X., Forveille, T., Perrier, C., & Mayor, M. 1998, A&A, 331, 581

Endal, A., & Sofia, S. 1981, ApJ, 243, 625

García-López, R. J., Rebolo, R., & Martín, E. L. 1994, A&A, 282, 518

Gliese, W. 1969, Catalogue of Nearby Stars, Veröff Astron. Rechen-Inst., Heidelberg, No. 22

Green, E. M., Demarque, P., & King, C. R. 1987, The Revised Yale Isochrones and Luminosity Functions, Yale University Observatory

Guenther, D. B., Demarque, P., Kim, Y.-C., & Pinsonneault, M. H. 1992, ApJ, 387, 372

Hambly, N., Hawkins, M. R. S., & Jameson, R. 1993, A&AS, 100, 607

Haro, G., Chavira, E., & González, G. 1982, Boll. Inst. Tonantzintla, 3, 3

Hartmann, L., Hewett, R., Stahler, S., & Mathieu, R. 1986, ApJ, 309, 275

Hertzsprung, E. 1947, Ann. Leiden Obs. 19, 1A

Jeffries, R. D., & Tolley, A. J. 1998, MNRAS, 300, 331

Jones, B. F. 1973, A&AS, 9, 313

Jones, B. F., Fischer, D., Shetrone, M., & Soderblom, D. R. 1997, AJ, 114, 352

Jones, B. F., Fischer, D., & Stauffer, J. 1996, AJ, 112, 1562

Kawaler, S. D. 1988, ApJ, 333, 236

Kearns, K. E., Eaton, N. L., Herbst, W., & Mazzurco, C. J. 1997, AJ, 114, 1098

Kearns, K. E., & Herbst, W. 1998, AJ, 116, 261

Keppens, R., MacGregor, K., & Charbonneau, P. 1995, A&A, 294, 469

Kirkpatrick, J. D., Kelly, D. M., Rieke, G. H., Leibert, J., Allard, F., & Wehrse, R. 1993, ApJ, 402, 643

Königl, A. 1991, ApJ, 370, L39

Kraft, R. 1967, in Spectroscopic Astrophysics, ed. G. Herbig (Berkeley: Univ. of Calif.), p. 385

Krishnamurthi, A., et al. 1998, ApJ, 493, 914

Krishnamurthi, A., Pinsonneault, M. H., Barnes, S., & Sofia, S. 1997, ApJ, 480, 303

Leggett, S. K., Allard, F., Berriman, G., Dahn, C. C., & Hauschildt, P. H. 1996, ApJS, 104, 117

Li, J., & Cameron, A. C. 1993, MNRAS, 261, 766

Luyten, W. J., Hill, G., & Morris, S. 1981, Proper Motions with the 48-inch Schmidt Telescope, LIX, Minnesota University Press

MacGregor, K., & Brenner, M. 1991, ApJ, 376, 204

Marcy, G., & Benitz, K. 1989, ApJ, 344, 441

Marcy, G., & Chen, G. H. 1992, ApJ, 390, 550

Meynet, G., Mermilliod, J.-C., & Maeder, A. 1992, A&AS, 98, 477

Monet, D. G., Dahn, C. C., Vrba, F. J., Pier, J. R., Luginbuhl, C. B., & Ables, H. D. 1992, AJ, 103, 638

Narayanan, V. K., & Gould, A. 1999, ApJ, 515, 256

Noyes, R. W., Hartmann, L. W., Baliunas, S. L., Duncan, D. K., & Vaughn, A. H. 1984, ApJ, 279, 763

Oppenheimer, B., Basri, G., Nakajima, T., & Kulkarni, S. 1997, AJ, 113, 296

Palla, F. & Stahler, S. W., 1991, ApJ, 375, 288

Patten, B., & Simon, T. 1996, ApJS, 106, 489

Perryman, M. A. C., et al. 1998, A&A, 331, 81

Pinsonneault, M. H., et al. 2000, in preparation

Pinsonneault, M., Kawaler, S., & Demarque, P. 1990, ApJS, 74, 501

Pinsonneault, M. H., Stauffer, J., Soderblom, D. R., King, J. R., & Hanson, R. 1998, ApJ, 504, 170

Queloz, D., Allain, S., Mermilliod, J.-C., Bouvier, J., & Mayor, M. 1998, A&A, 335, 183

Radick, R., Thompson, D., Lockwood, G., Duncan, D. & Baggett, W. 1987, ApJ, 321, 459

Reid, N. 1991, MNRAS, 257, 257

Saumon, D., Chabrier, G., & Van Horn, H. M. 1995, ApJS, 99, 713

Sills, A., Pinsonneault, M. H., & Terndrup, D. M. 1999, ApJ, submitted

Skumanich, A. 1972, ApJ, 171, 565

Slettebak, A. 1956, ApJ, 124, 173

Soderblom, D., Stauffer, J., Hudon, D., & Jones, H. 1993, ApJS, 85, 315

Stassun, K. G., Mathieu, R. D., Mazeh, T., & Vrba, F. J. 1999, AJ, 117, 2941

Stauffer, J. R., Balachandran, S. C., Krishnamurthi, A., Pinsonneault, M., Terndrup, D. M., & Stern, R. A. 1997, ApJ, 475, 604

Stauffer, J., Giampapa, M., Stern, R., Herbst, W., & Hartmann, L. 1991, ApJ, 374, 142

Stauffer, J. R., Hamilton, D., & Probst, R. G. 1994, AJ, 108, 155

Stauffer, J., & Hartmann, L. W. 1987, ApJ, 318, 337

Stauffer, J., Hartmann, L. W., Burnham, J. M., & Jones, B. F. 1985, ApJ, 289, 247

Stauffer, J., Hartmann, L. W., Jones, B., & McNamara, B. 1989, ApJ, 342, 285

Stauffer, J., Hartmann, L. W., & Latham, D. W. 1987, ApJ, 320, L51

Stauffer, J., Hartmann, L., Prosser, C., Randich, S., Balachandran, S., Patten, B., Simon, T., & Giampapa, M. 1997, ApJ, 479, 776

Stauffer, J., Hartmann, L., Soderblom, D. R., & Burnham, N. 1984, ApJ, 280, 202

Stauffer, J., Klemola, A., Prosser, C., & Probst, R. 1991, AJ, 101, 980

Stauffer, J. R., Liebert, J., & Giampapa, M. 1995, AJ, 109, 298

Stauffer, J. R., Schild, R., Barrado y Navascués, D., Backman, D. E., Angelova, A. M., Kirkpatrick, J. D., Hambly, N., & Vanzi, L. 1998, ApJ, 504, 820

Stauffer, J. R., Shultz, G., & Kirkpatrick, J. D. 1998, ApJ, 499, L199

Stefanik, R. P., & Latham, D. W. 1985, in Stellar Radial Velocities, IAQ Colloq. 88, eds. A. G. D. Philip & D. W. Latham (Schnectady: L. Davis Press), 213

Terndrup, D. M., Krishnamurthi, A., Pinsonneault, M., & Stauffer, J. R. 1999, AJ, in press

Thompson, M. J., et al. 1996, Science, 272, 1300

Thorburn, J. A., Hobbs, L. M., Deliyannis, C. P., & Pinsonneault. M. H. 1993, ApJ, 415, 150

Vogt, S. S., et al. 1994, Proc. SPIE, 2198, 362

Weber, E. J., & Davis, L. 1967, ApJ, 148, 217

Wolff, S. C., & Simon, T. 1997, PASP, 109, 759

Young, A., Skumanich, A., Stauffer, J., Hartmann, L., Bopp, B., & Harlan, G. 1989, ApJ, 344, 427

Ziskin, V. 1993, Senior thesis, Harvard University.

Fig. 1.— Examples of spectra at Hα (left panels) and near 8400 Å (right) for stars in the Pleiades, ordered from top to bottom by decreasing $v \sin i$.

Fig. 2.— Same as Figure 1, but for three stars in the Hyades.

Fig. 3.— Radial velocities of M stars in the Pleiades (upper panel) and the Hyades (lower panel). Open circles denote stars with measured $v \sin i$, while triangles indicate upper limits. The dashed line in each panel shows the mean velocity of large samples of stars in the Pleiades (Narayanan & Gould 1999) and in the Hyades (Perryman et al. 1998). As discussed in the text, errors in each point are better than 1 km s^{-1} for slowly rotating stars, but are about 10% of the $v \sin i$ value for rapidly rotating stars.

Fig. 4.— Color-magnitude diagram for the Pleiades and comparison to model isochrones. The photometry has been dereddened using $E(B-V) = 0.04$. The long dashed line shows the YREC models for an age of 110 Gyr and using the Yale color calibration (Green et al. 1987), shifted to a distance modulus of 5.6. The solid line shows the empirical isochrone for the Pleiades, derived as discussed in the text. The YREC models were adjusted by altering the color-temperature relation so that they matched the empirical isochrone.

Fig. 5.— Same as Figure 4, but in $(V-I)_0$. Open circles show photometry in the Pleiades which have previous measures of $v \sin i$, while the triangles are photometry for the stars observed in this paper.

Fig. 6.— Comparison of color-temperature scales in (upper panel) $V-I_C$ and (lower panel) $B-V$. The solid lines show the effective temperature at each color from the empirical isochrone for the Pleiades. The dashed line in the lower panel is from Soderblom et al. (1993), while that in the upper panel is that employed by Stauffer et al. (1997b), based on data in Kirkpatrick et al. (1993) and color transformations by Bessell (1979). The solid points in $V-I$ are for some individual M dwarfs in Kirkpatrick et al. (1993), while the open points with error bars are for stars in Leggett et al. (1996).

Fig. 7.— Data on rotation rates in (top) the Pleiades and (bottom) the Hyades. Filled points are from this study, while open points are from other papers as described in the text. Limits are shown as downward pointing triangles. The numbers at the bottom of each panel show the equivalent masses from the empirical isochrone in solar units, derived as discussed in the text.

Fig. 8.— Distribution of rotation rates for three intervals of effective temperature. The solid line shows the number of stars in equal intervals of $\log_{10} v \sin i$ for the Pleiades. The dashed line in the lower panel shows the distribution of rotation rates for the low-mass stars in the Hyades.

Fig. 9.— Width of Hα emission plotted against color. Filled symbols are for the Hyades sample in this paper plus a few points from Jones et al. (1996); these are shown as upward- and downward-pointing triangles, respectively. Open circles are for Pleiades stars in this paper, while crossed open

circles are from Jones et al. (1996).

Fig. 10.— Correlation between rotation and Hα width. Symbols are the same as in Figure 9. The data have been divided into mass bins using the mass estimates derived as described in the text. Points with upper limits to $v \sin i$ are plotted at that limit.

Fig. 11.— Cumulative distribution $F(v \sin i)$ of rotation rates in the Hyades (thick line) compared to that for the Pleiades at an age of 600 Myr (thin line), computed from the observed velocities as described in the text.

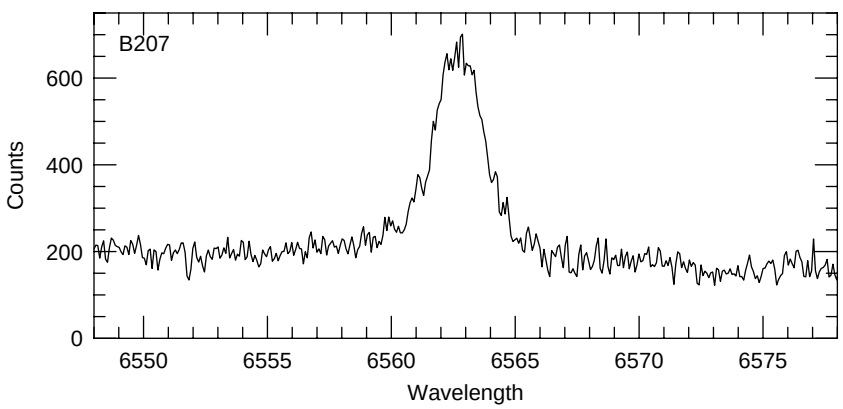
B207
Counts
Wavelength
0
200
400
600
6550
6555
6560
6565
6570
6575

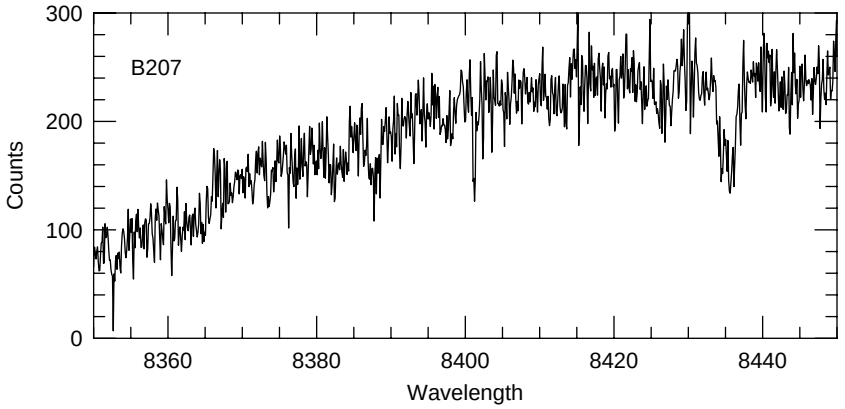
B207
Counts
Wavelength
0
100
200
300
8360
8380
8400
8420
8440

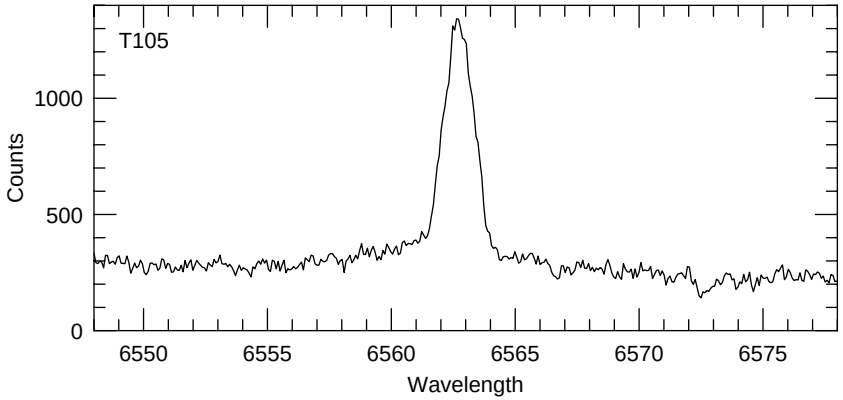
T105
Counts
Wavelength
0
500
1000
6550
6555
6560
6565
6570
6575

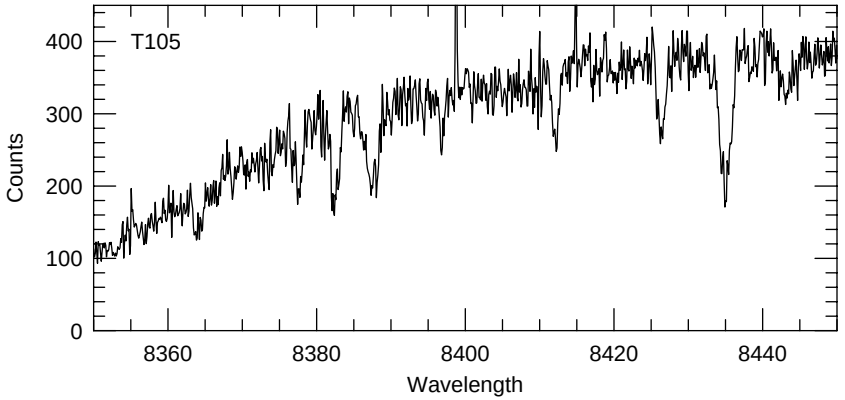
T105
Counts
Wavelength
0
100
200
300
400
8360
8380
8400
8420
8440

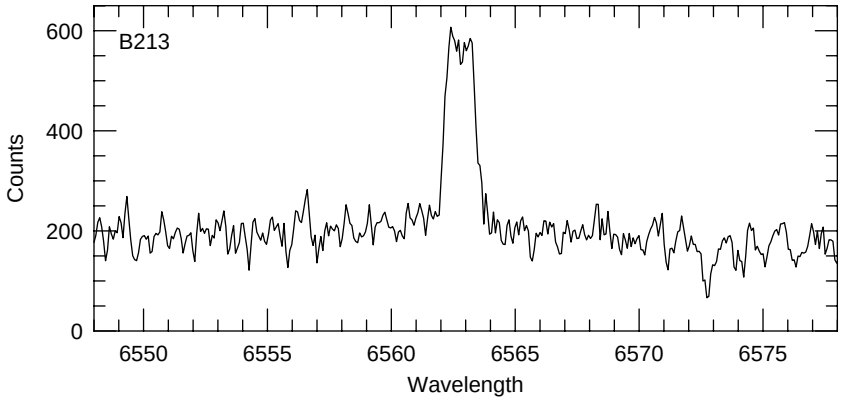
B213
Counts
Wavelength
0
200
400
600
6550
6555
6560
6565
6570
6575

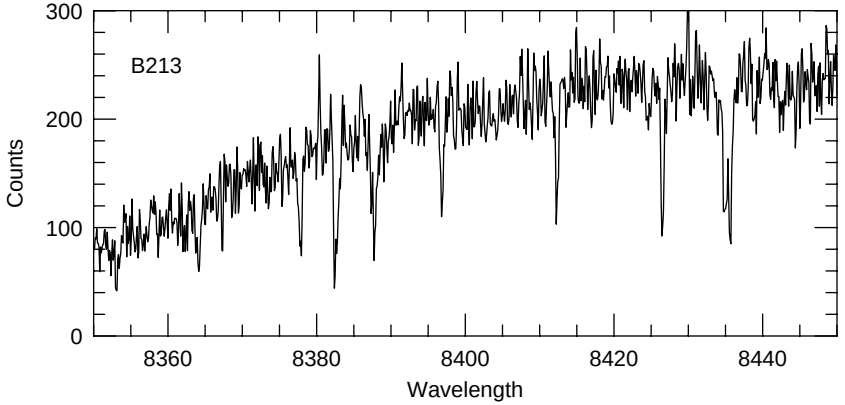
B213
Counts
Wavelength
0
100
200
300
8360
8380
8400
8420
8440

TABLE 1. KPNO observations in the Pleiades

HCG	$V-I_C$	$v \sin i$ (km s^{-1})	v_r (km s^{-1})	$W(H\alpha)$ (Å)	T	SK	HHJ	Other designation
20	1.73	10	5.6	1.0	1B			
55	2.60	< 7	5.8	1.9		705		B346
58	2.03	93	6.0	3.1	35			
68	2.51	40	5.0	4.0	36	697	396	
71	1.82	10	5.6	1.4				B256
75	1.81	8	5.7	0.7		684		B289
77	2.09	50	5.0	2.8		681		A80
80	2.36	69	4.0	4.4	3	673	409	J8
100	2.64	11	10.0	3.3	40	654	383	
118	1.77	16	6.5	1.5	39B	625		HII133
121	1.80	11	7.6	0.9	149	631		HII146
126	2.44	75	6.0	4.2	69	600	391	
127	1.83	9	6.3	0.7		606		HII191
134	2.24	7	6.1	2.7	150	591		
141	2.22	44	9.0	3.5	71	590		
142	2.47	21	7.4	3.7	10	561		
143	2.56	37	5.2	9.1	19B	568	348	
150	2.65	13	6.2	6.6		567	364	B179
154	1.93	80	7.0	1.3	160			HII347
161	2.56	13	6.0	3.7		559	344	A23=A57
179	1.72	< 7	5.9	0.3	45	524		
181	2.48	26	7.0	5.1			405	B196
195	2.30	65	2.0	3.6	78			
209	2.39	15	3.9	4.1		482		HII906
219	2.46	65	3.0	5.2			429	A2
222	1.75	< 7	6.1	0.0		472		B212
224	1.82	< 7	5.6	0.7	469			HII1061
231	1.80	8	4.8	0.9	44B	463		
241	2.43	< 7	5.7	2.7		453		B267
248	2.73	43	7.8	5.7		443	390	B180
249	1.84	85	3.0	2.5	27B			
258	2.47	42	9.3	5.6		437		B363
262	1.88	13	6.0	1.0				HII1355
274	1.82	< 7	7.7	1.4	30B	429		
275	2.76	26	7.8	6.7	18			
277	2.58	27	9.2	5.9	105	413	424	
280	1.71	50	8.0	1.3				B271
298	2.44	39	9.1	4.5	83	399	433	
309	2.42	10	7.6	3.5	154	385	375	
313	2.98	23	10.2	9.2	23	371		
319	2.23	13	4.4	3.0	51	369		HII1827
323	2.47	19	6.9	3.4		370	373	A91
339	2.57	64	-5.0	6.2		349		B207
341	1.88	8	6.7	0.6	87			
353	2.16	< 7	6.5	1.2		336		A55
354	2.36	20	6.8	3.4	157	331		
372	2.60	7	6.6	5.6	90	372	346	

TABLE 1. (continued)

HCG	$V - I_C$	$v \sin i$ (km s^{-1})	v_r (km s^{-1})	$W(\mathrm{H}\alpha)$ (Å)	T	SK	HHJ	Other designation
380	2.52	< 7	7.1	2.7	92	294		
403	2.57	< 7	5.8	2.3		272		B213
423	1.97	53	6.0	2.6	95	239		
430	1.64	< 7	6.7	0.1		229		HII3030
427	2.44	< 7	6.6	3.8	29	232		
454	2.17	75	0.0	2.9	159	188		
477	1.78	105	0.0	2.5	61	106		
491	2.17	27	5.7	2.3				B127
499	2.01	32	7.7	2.0	99			
...	1.63	< 7	6.5	0.0		378		HII1756
...	1.63	< 7	7.8	0.2				HII2548
...	1.72	18	6.7	0.8				HII930

Notes to Table 1.

Star identifications: HCG = Haro et al. (1982); SK = Stauffer et al. (1991b); HHJ = Hambley et al. (1993); A, B, T = Asiago, Byurakan, Tacubaya (referenced in Jones 1981); J = Jones (1973).

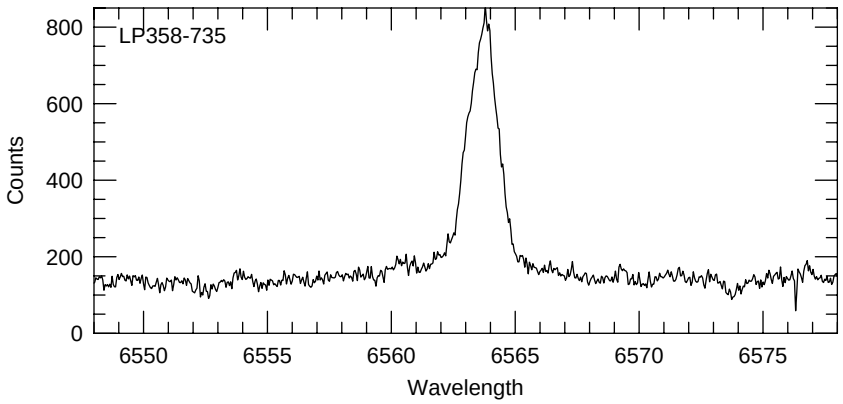
LP358-735
Counts
Wavelength
0
200
400
600
800
6550
6555
6560
6565
6570
6575

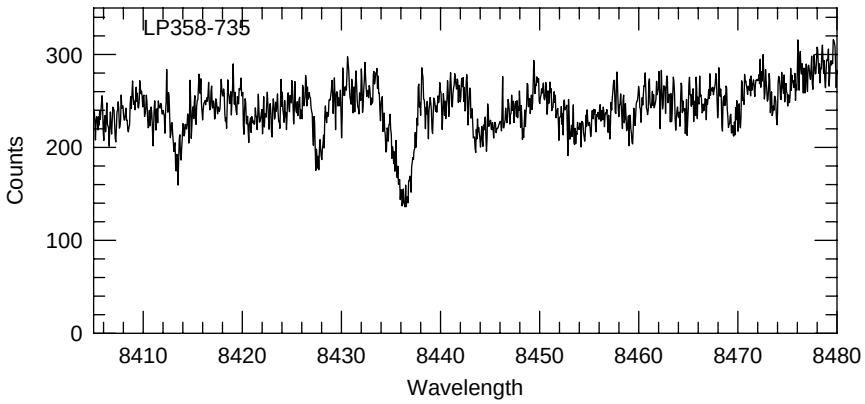
LP358-735
Counts
Wavelength
0
100
200
300
8410
8420
8430
8440
8450
8460
8470
8480

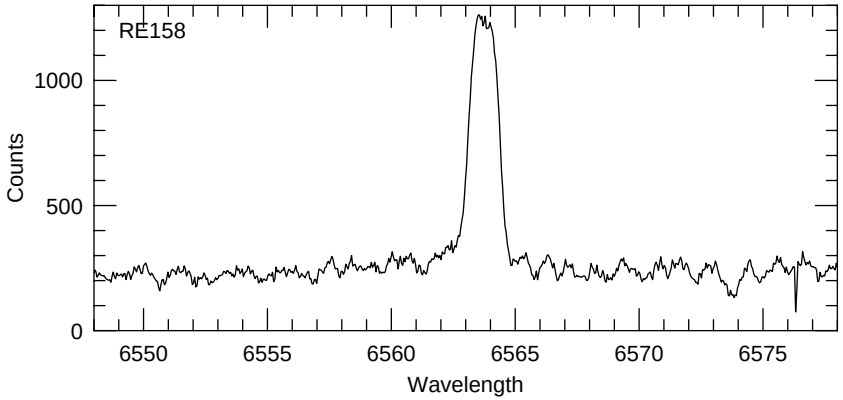
RE158
Counts
Wavelength
0
500
1000
6550
6555
6560
6565
6570
6575

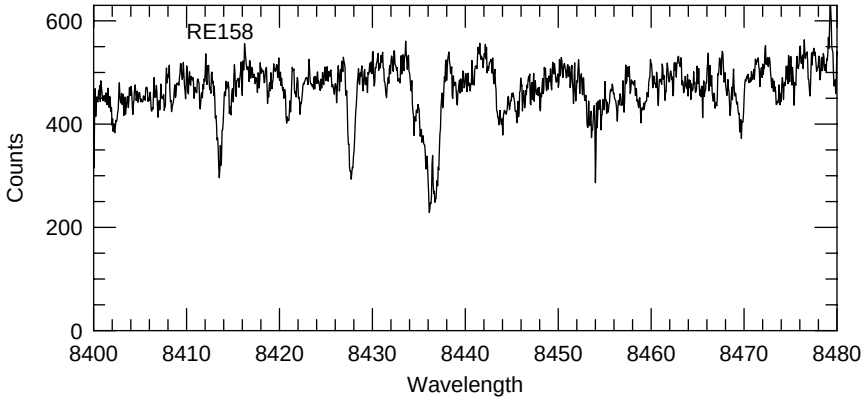
RE158
Counts
Wavelength
0
200
400
600
8400
8410
8420
8430
8440
8450
8460
8470
8480

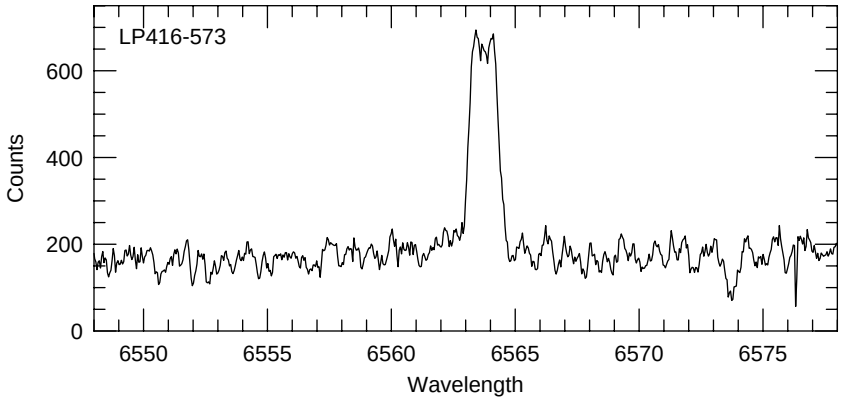
LP416-573
Counts
Wavelength
0
200
400
600
6550
6555
6560
6565
6570
6575

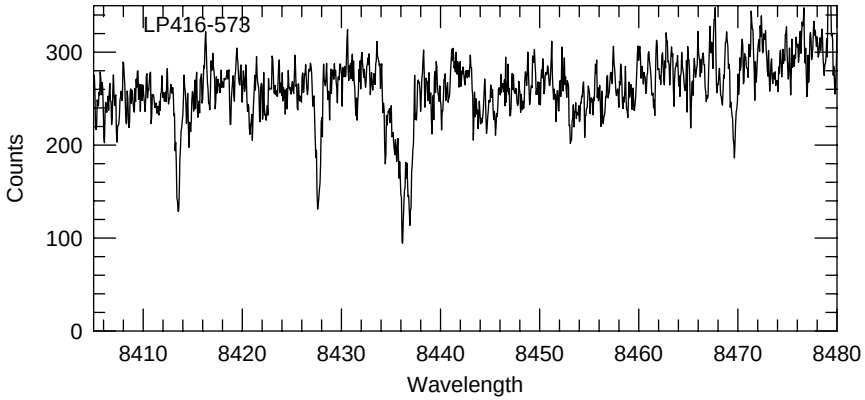
LP416-573
Counts
Wavelength
0
100
200
300
8410
8420
8430
8440
8450
8460
8470
8480

TABLE 2. Keck Pleiades data

Star	$V - I_C$	$v \sin i$ (km s^{-1})	v_r (km s^{-1})	$W(\mathrm{H}\alpha)$ (Å)	Other designation	Note
HHJ92	3.63	16.	4.9	4.5		
HHJ292E	2.9:	16.	6.2	6.1		
HHJ297	2.8:	8.	···	5.7		SB2
HHJ300	2.5:	$< 7.$	5.5	2.6		
HHJ303	2.9:	24.	4.9	4.5		SB2?
HHJ305	2.2:	$< 7.$	4.6	1.1		
HHJ310	2.5:	20.	5.4	4.8		
HHJ373	2.47	20.	7.0	3.0	HCG323, Sk370, A91	
HHJ374	2.46	$< 7.$	6.4	1.7		
HHJ375	2.42	10.	6.5	2.5	HCG309, Sk385, T154	
HHJ377	2.4:	20.5	5.7	4.3		
HHJ381	2.3:	8.	5.0	2.3		

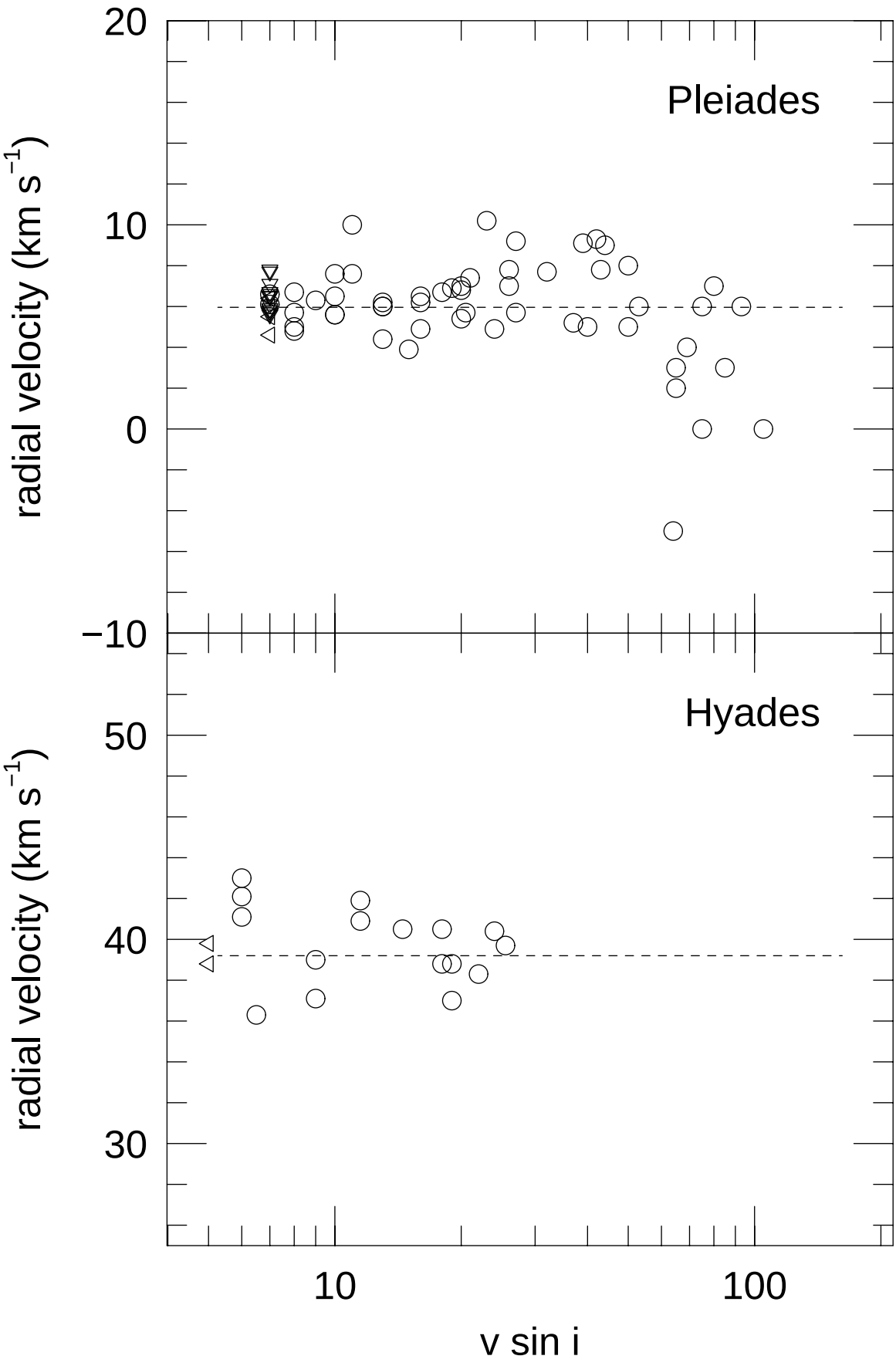
Pleiades
Hyades
radial velocity (km s^{-1})
radial velocity (km s^{-1})
20
10
0
−10
50
40
30
10
100
v sin i

TABLE 3. Hyades data

Star	$V - I_C$	$v \sin i$ (km s^{-1})	v_r (km s^{-1})	W(Hα) (Å)	Other designation
Re158	3.20	11.5	40.9	5.4	LP475-14
Re128	3.39	19.	38.8	4.9	LP474-221
Re240b	3.82	14.5	40.5	4.4	
Re390	3.83	18.	40.5	8.5	LP415-1773
Re115	3.08	9.	39.0	3.0	
LP416-573	3.03	6.	42.1	2.8	
LP358-735	3.21	25.5	39.7	5.4	
LP476-648	2.95	6.	43.0	3.0	
LP358-717	3.11	18.	38.8	3.8	
Re346	3.09	6.	41.1	2.7	LP475-116
Re119	3.59	9.	37.1	2.7	LP414-138
Re23	2.94	6.5	36.3	3.1	LP414-30
Re206	3.09	24.	40.4	3.6	LP475-56
Re138	3.62	22.	38.3:	6.6	LP414-2008
Re60	3.12	19.	37.0:	4.2	LP474-1100
Re386	3.76	11.5	41.9	4.5	LP415-2128
Bry358	3.56	$< 5.$	39.8	7.0	
Re202	3.33	$< 5.$	38.8	2.8	LP415-51

Notes to Table 3.

Star identifications: Bry = Bryja et al. (1994); LP = Luyten et al. (1981); Re = Reid (1992).

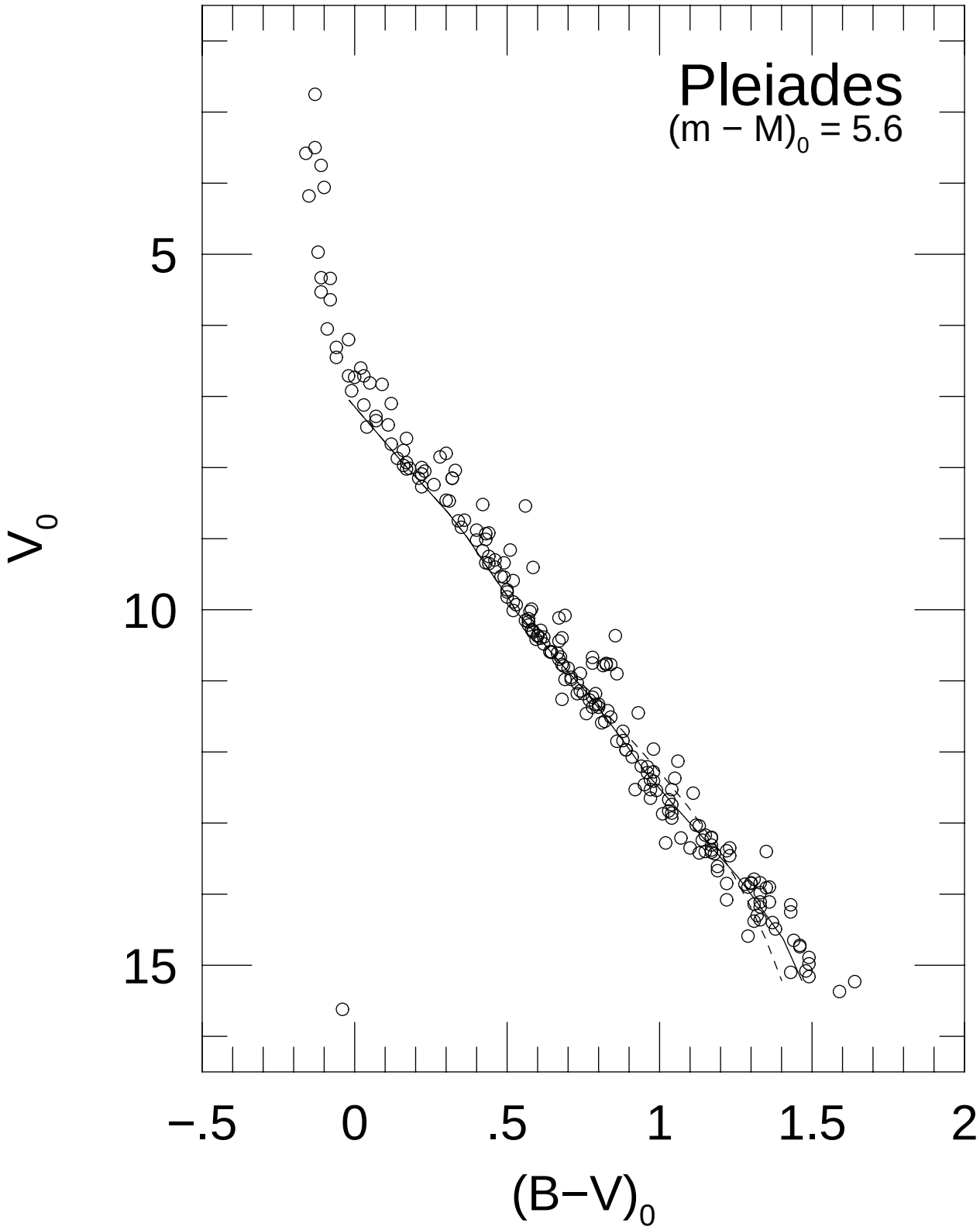
Pleiades
(m − M)0 = 5.6
5
10
15
V0
−.5
0
.5
1
1.5
2
(B−V)0

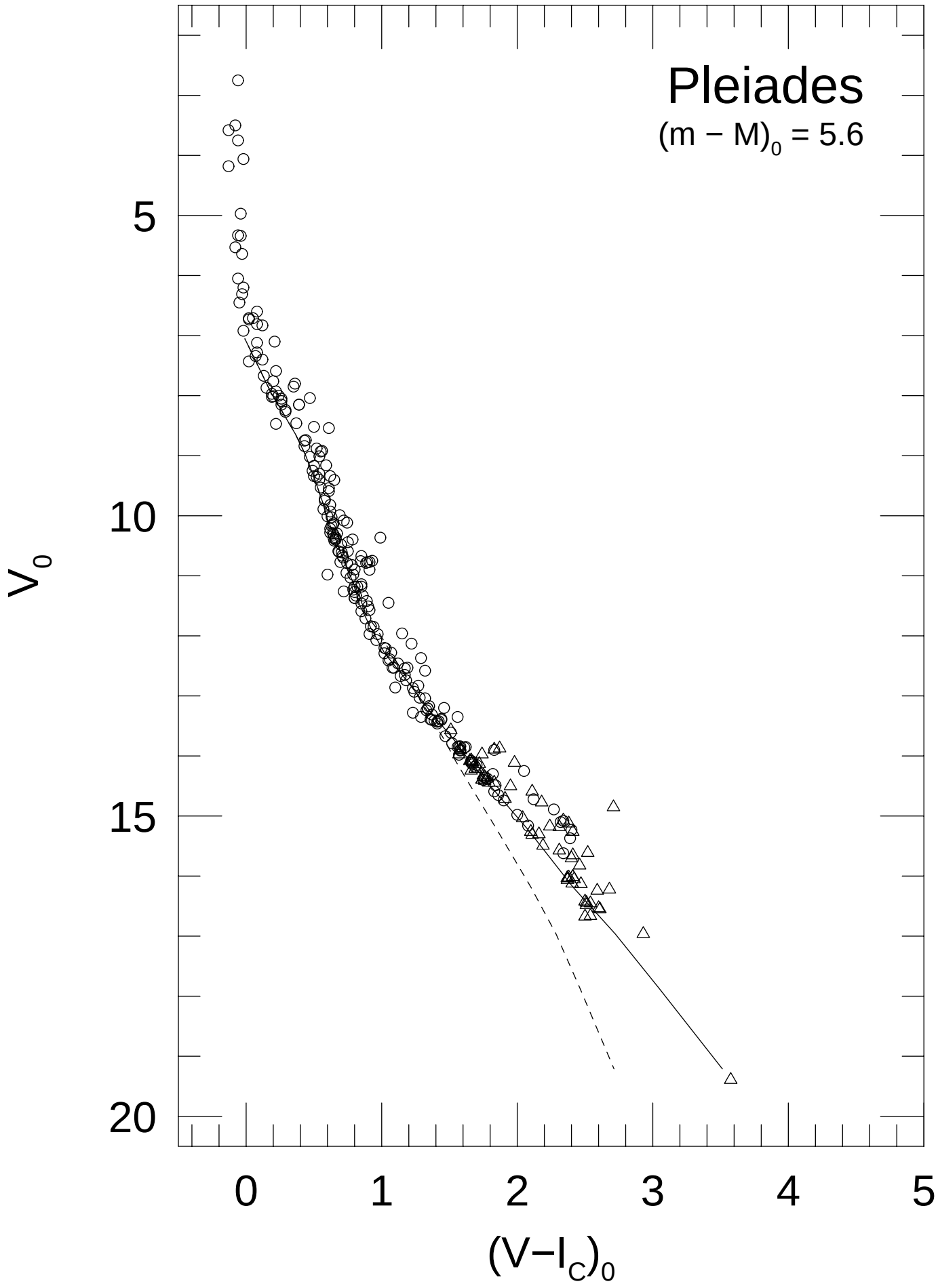
Pleiades
(m − M)0 = 5.6
5
10
15
20
V0
0
1
2
3
4
5
(V−IC)0

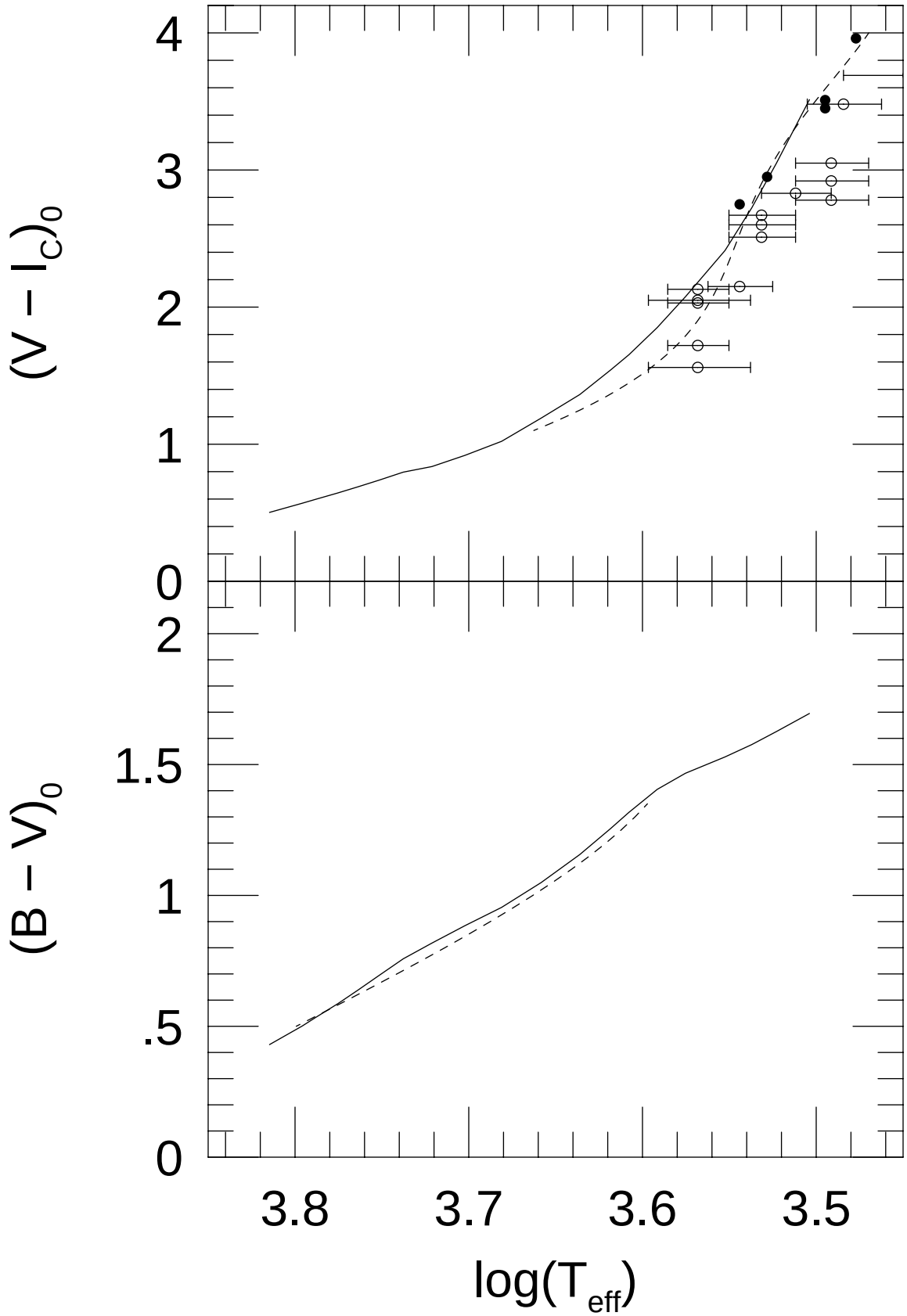
4
3
2
1
0
$(V - I_C)_0$
2
1.5
1
.5
0
$(B - V)_0$
3.8
3.7
3.6
3.5
$\log(T_{eff})$

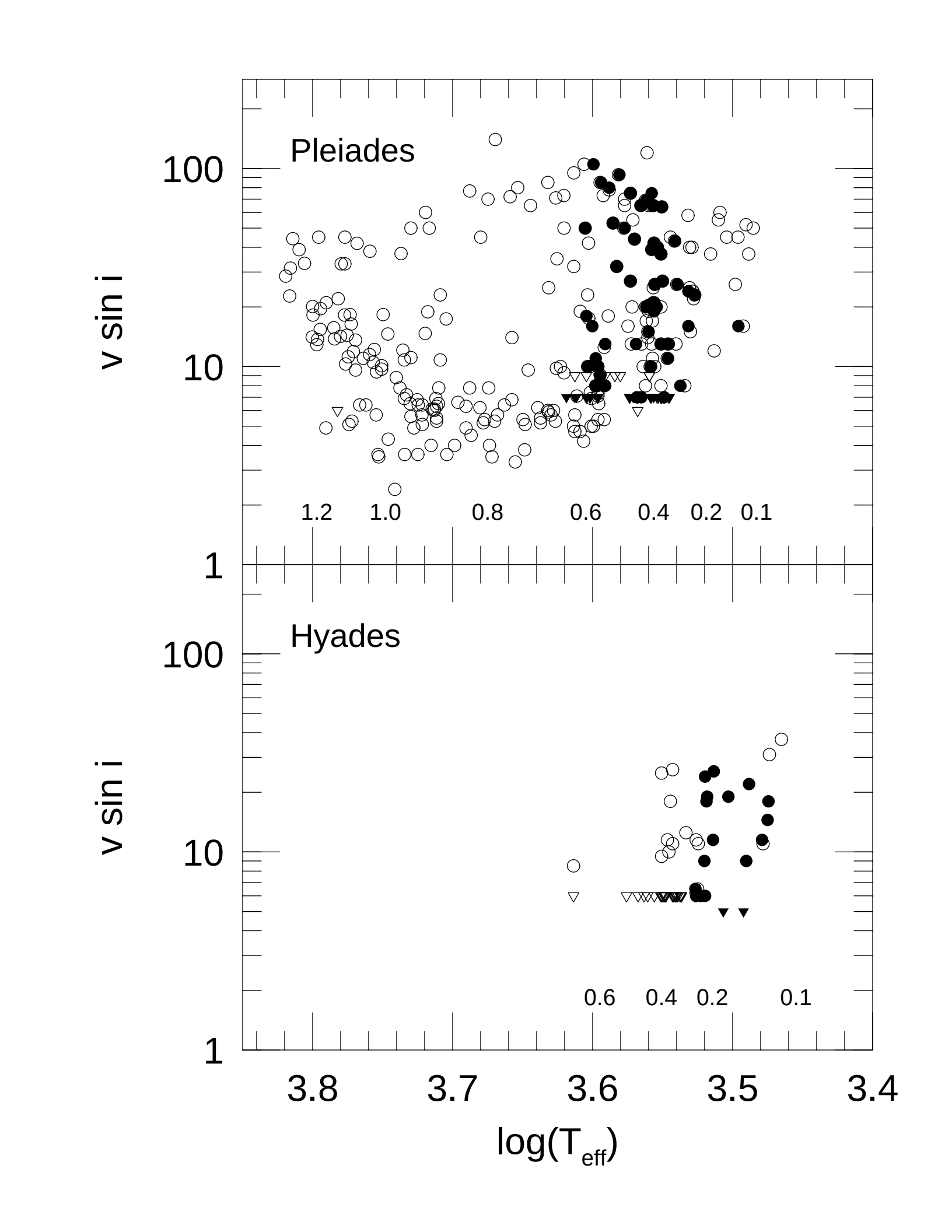
Pleiades
Hyades
v sin i
v sin i
100
10
1
100
10
1
1.2
1.0
0.8
0.6
0.4
0.2
0.1
0.6
0.4
0.2
0.1
3.8
3.7
3.6
3.5
3.4
log(T_eff)

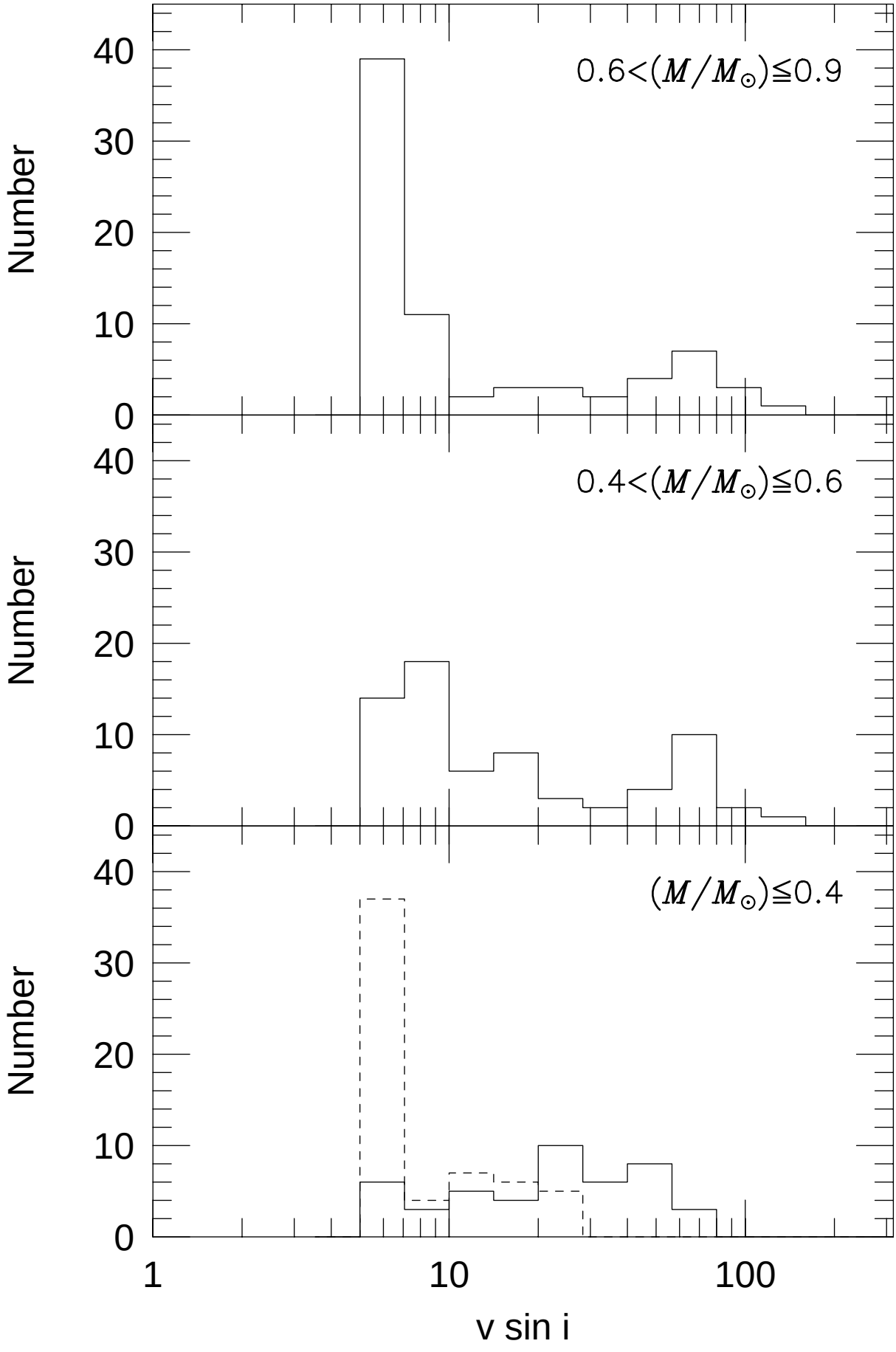
0.6<(M/M⊙)≦0.9
0.4<(M/M⊙)≦0.6
(M/M⊙)≦0.4
Number
Number
Number
0
10
20
30
40
1
10
100
v sin i

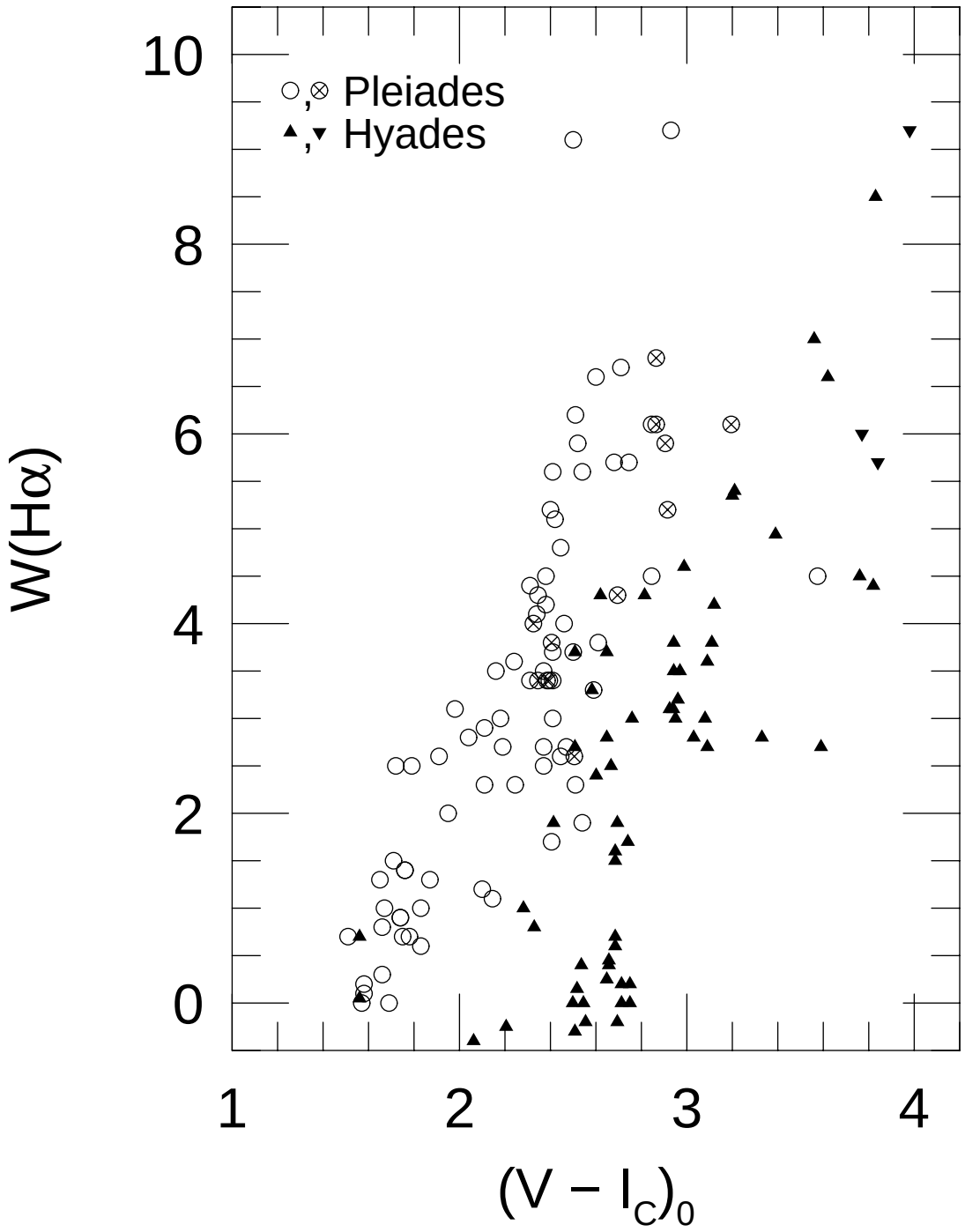
Pleiades
Hyades
W(Hα)
(V − I_C)_0
0
2
4
6
8
10
1
2
3
4

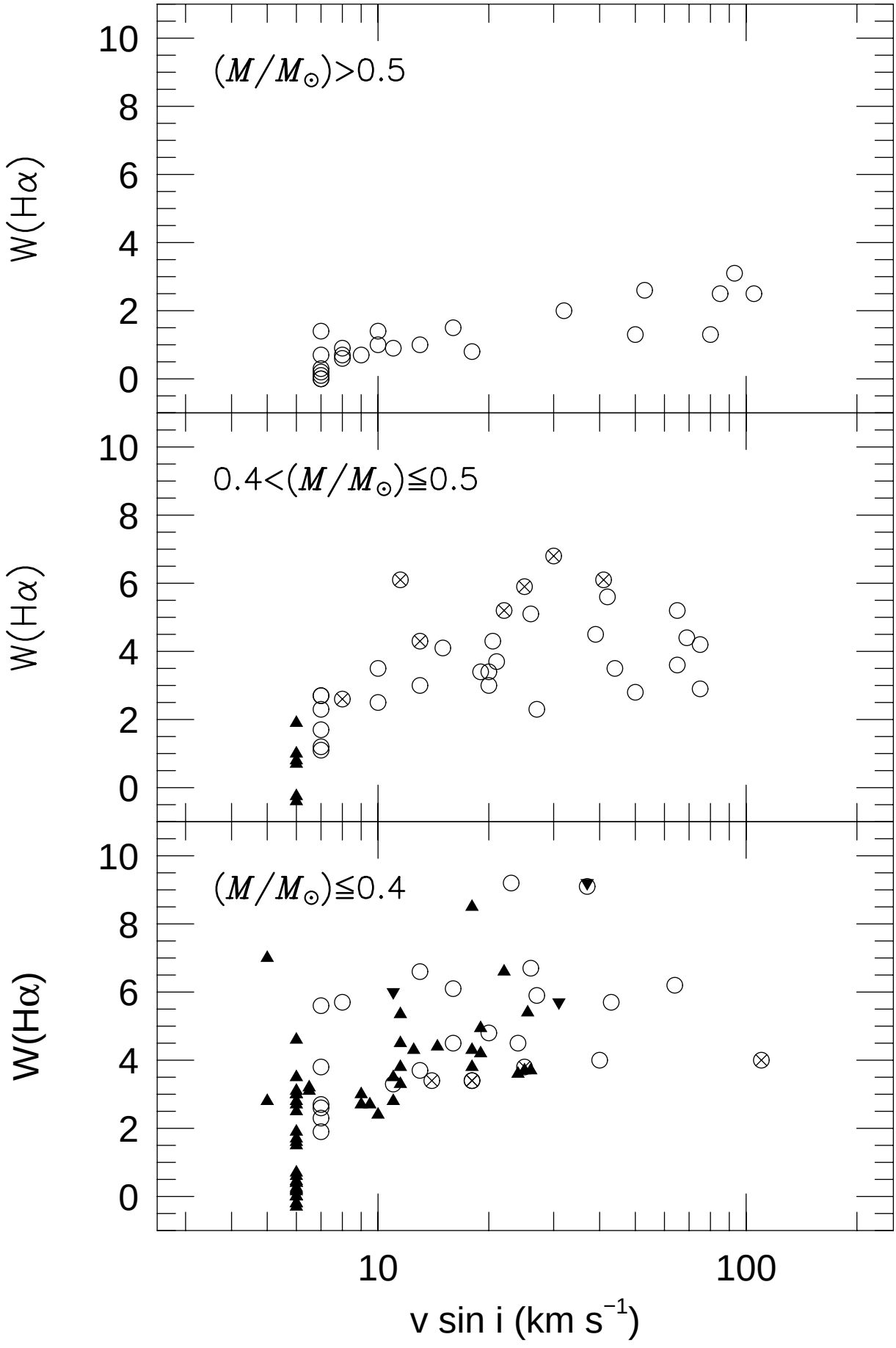
$(M/M_\odot)$>0.5
0.4<$(M/M_\odot)$≦0.5
$(M/M_\odot)$≦0.4
W(Hα)
W(Hα)
W(Hα)
10
8
6
4
2
0
10
8
6
4
2
0
10
8
6
4
2
0
10
100
v sin i (km s^{-1})

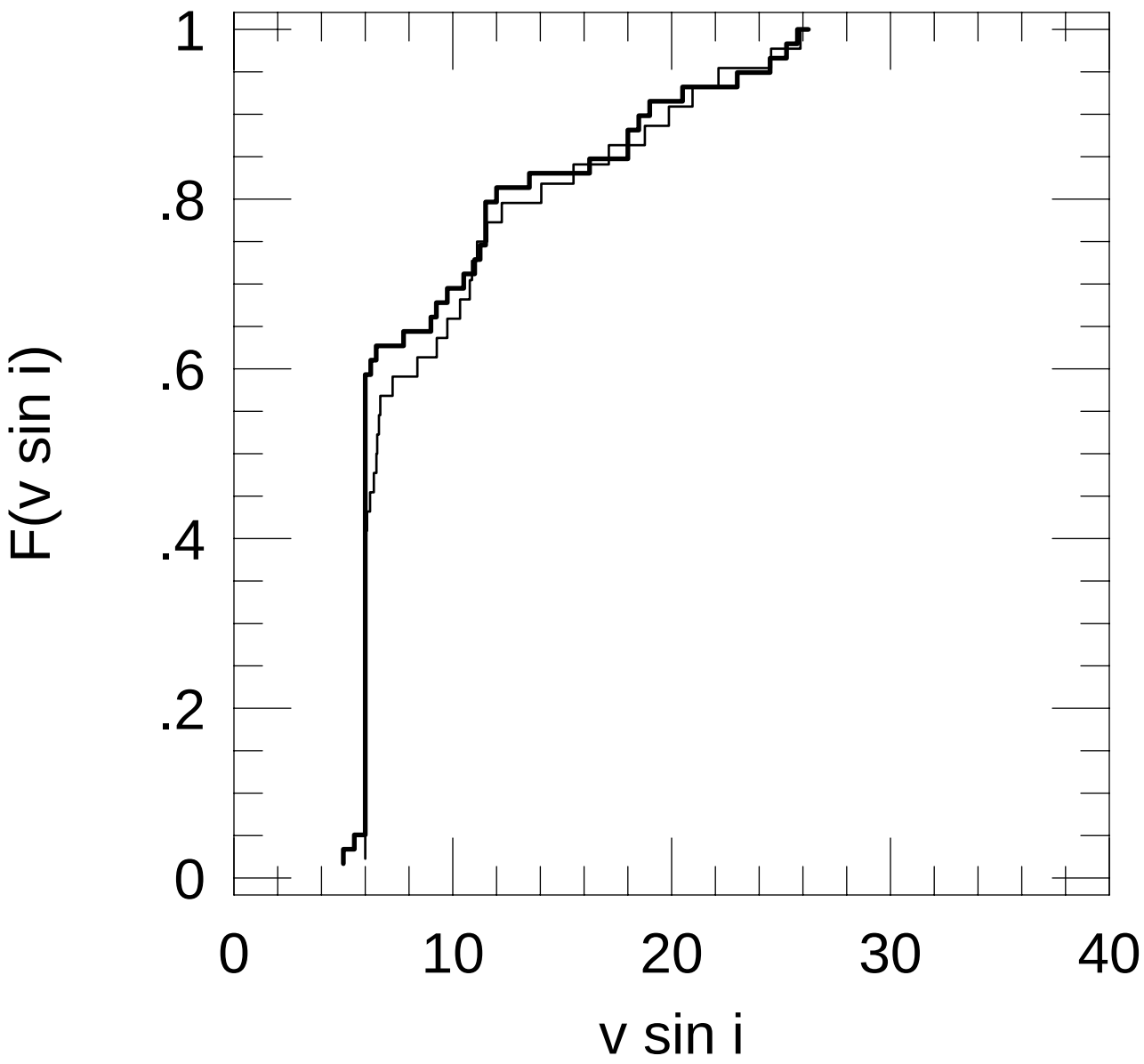
1
.8
.6
.4
.2
0
F(v sin i)
0
10
20
30
40
v sin i